NAVAL POSTGRADUATE SCHOOL

MONTEREY, CALIFORNIA

THESIS

VIABILITY OF CROSS-FLOW FAN WITH HELICAL BLADES FOR VERTICAL TAKE-OFF AND LANDING AIRCRAFT

by

Howe Leng Kwek

September 2012

Thesis Advisor:	Garth V. Hobson
Second Reader:	Anthony J. Gannon

Approved for public release; distribution is unlimited

THIS PAGE INTENTIONALLY LEFT BLANK

REPORT DOCUMENTATION PAGE			Form Approved OMB No. 0704-0188
Public reporting burden for this collection of information is estimated to average 1 hour per response, including the time for reviewing instruction, searching existing data sources, gathering and maintaining the data needed, and completing and reviewing the collection of information. Send comments regarding this burden estimate or any other aspect of this collection of information, including suggestions for reducing this burden, to Washington headquarters Services, Directorate for Information Operations and Reports, 1215 Jefferson Davis Highway, Suite 1204, Arlington, VA 22202-4302, and to the Office of Management and Budget, Paperwork Reduction Project (0704-0188) Washington DC 20503.			
1. AGENCY USE ONLY ***(Leave blank)***	**2. REPORT DATE** September 2012	**3. REPORT TYPE AND DATES COVERED** Master's Thesis	
4. TITLE AND SUBTITLE Viability of Cross-Flow Fan with Helical Blades for Vertical Take-off and Landing Aircraft		**5. FUNDING NUMBERS**	
6. AUTHOR(S) Howe Leng Kwek			
7. PERFORMING ORGANIZATION NAME(S) AND ADDRESS(ES) Naval Postgraduate School Monterey, CA 93943-5000		**8. PERFORMING ORGANIZATION REPORT NUMBER**	
9. SPONSORING /MONITORING AGENCY NAME(S) AND ADDRESS(ES) N/A		**10. SPONSORING/MONITORING AGENCY REPORT NUMBER**	
11. SUPPLEMENTARY NOTES The views expressed in this thesis are those of the author and do not reflect the official policy or position of the Department of Defense or the U.S. Government. IRB Protocol number ___N/A____.			
12a. DISTRIBUTION / AVAILABILITY STATEMENT Approved for public release; distribution is unlimited		**12b. DISTRIBUTION CODE**	

13. ABSTRACT (maximum 200 words)

The cross-flow fan (CFF) is a lifting and propulsion device that retains the advantages of a fixed-wing aircraft by using a ducted lift fan. There is no upper limit to the rotor length-to-diameter ratio of a CFF, allowing the device to be installed along the length of the wing or lifting device. The CFF discharged vector can be easily rotated about the fan axis since the fan has no angular requirements, further allowing the capability of vertical take-off and landing (VTOL) by thrust vectoring. CFF possess the potential to propel an airframe to flight; however adequate thrust must be produced by the CFF in order for it to realize VTOL.

Conventional CFFs designs with straight blades produce unacceptable noise levels for personal air vehicle operation. It is believed that helical blades could solve the sound pressure level problem and produce more thrust to aid VTOL. Using computational fluid dynamics (CFD) software, ANSYS-CFX, a three-dimensional (3-D) straight-bladed model was validated against previous study's experimental results.

A 3-D model with helical blades was constructed to investigate the performance. The analytical results have shown that helical blades could increase the thrust performance of a CFF, and could possibly realize VTOL.

14. SUBJECT TERMS cross-flow fan (CFF), vertical take-off and landing (VTOL), straight blades, computational fluid dynamics (CFD), ANYSY-CFX, helical blades			**15. NUMBER OF PAGES** 70
			16. PRICE CODE
17. SECURITY CLASSIFICATION OF REPORT Unclassified	**18. SECURITY CLASSIFICATION OF THIS PAGE** Unclassified	**19. SECURITY CLASSIFICATION OF ABSTRACT** Unclassified	**20. LIMITATION OF ABSTRACT** UU

NSN 7540-01-280-5500 Standard Form 298 (Rev. 8-98)
Prescribed by ANSI Std. Z39.18

THIS PAGE INTENTIONALLY LEFT BLANK

Approved for public release; distribution is unlimited

VIABILITY OF CROSS-FLOW FAN WITH HELICAL BLADES FOR VERTICAL TAKE-OFF AND LANDING AIRCRAFT

Howe Leng Kwek
Major, Republic of Singapore Air Force
B.E., University of Queensland, 2001

Submitted in partial fulfillment of the
requirements for the degree of

MASTER OF SCIENCE IN ENGINEERING SCIENCE
(MECHANICAL ENGINEERING)

from the

NAVAL POSTGRADUATE SCHOOL
September 2012

Author: Howe Leng Kwek

Approved by: Garth V. Hobson
Thesis Advisor

Anthony J. Gannon
Second Reader

Knox T. Millsaps
Chair, Department of Mechanical and Aerospace Engineering

THIS PAGE INTENTIONALLY LEFT BLANK

ABSTRACT

The cross-flow fan (CFF) is a lifting and propulsion device that retains the advantages of a fixed-wing aircraft by using a ducted lift fan. There is no upper limit to the rotor length-to-diameter ratio of a CFF, allowing the device to be installed along the length of the wing or lifting device. The CFF discharged vector can be easily rotated about the fan axis since the fan has no angular requirements, further allowing the capability of vertical take-off and landing (VTOL) by thrust vectoring. CFF possess the potential to propel an airframe to flight; however adequate thrust must be produced by the CFF in order for it to realize VTOL.

Conventional CFFs designs with straight blades produce unacceptable noise levels for personal air vehicle operation. It is believed that helical blades could solve the sound pressure level problem and produce more thrust to aid VTOL. Using computational fluid dynamics software (CFD), ANSYS-CFX, a three-dimensional (3-D) straight-bladed model was validated against previous study's experimental results.

A 3-D model with helical blades was constructed to investigate the performance. The analytical results have shown that helical blades could increase the thrust performance of a CFF, and could possibly realize VTOL.

THIS PAGE INTENTIONALLY LEFT BLANK

TABLE OF CONTENTS

THIS PAGE INTENTIONALLY LEFT BLANK

LIST OF FIGURES

LIST OF TABLES

THIS PAGE INTENTIONALLY LEFT BLANK

LIST OF ACRONYMS AND ABBREVIATIONS

2-D	Two-dimensional
3-D	Three-dimensional
ANSYS-CFX	The CFD simulation program in ANSYS Workbench. It is divided into CFX-Pre, CFX-Solver, and CFD-Post. It uses an implicit solver and can run both steady-state and transient simulations.
ANSYS-CFX-Pre	The portion of CFX where boundary conditions and solver settings are selected. It was the first CFX program used while conducting a simulation.
ANSYS-CFX-Solver	The portion of CFX that runs the solver program, which gets its inputs from the set-up in CFX-Pre. It displays variable residuals as the solver is running.
ANSYS-MESHER	A mesh generation program inside ANSYS Workbench
ANSYS-WORKBENCH	A simulation package that includes a mesh generation program and CFX
CAD	Computer-aided drafting
*.def	The definition file created by ANSYS-CFX-Pre as required to run the simulation
CFD	Computational Fluid Dynamics
CFF	Cross-Flow Fan
CFD-POST	The portion of CFX that performs post-processing functions on the flow field data from the CFX-Solver.
dB	Decibels
ε	Viscous dissipation
h	Enthalpy
HVAC	Heating ventilation and cooling
k	Turbulent kinetic energy
k-ε	k-epsilon is the default turbulence model.
LTV	Ling-Temco-Vought was a large United States conglomerate which existed from 1969 to 2000.
μ	Dynamic viscosity
PARASOLID	A solid model file that can be opened in most solid modeling programs.
P	Pressure
Pa	Pascal
ρ	Density
rpm	Revolutions per minute
SOLIDWORKS	A solid modeling program in which DesignModeler is the

	module for constructing the models.
T	Temperature
TPL	Turbopropulsion Laboratory
U	Velocity
VTOL	Vertical take-off and landing
VSD	Vought Systems Division

ACKNOWLEDGMENTS

A sincere thank you is given to the faculty and staff at the M. H. Vavra Turbopropulsion Laboratory (TPL). I have greatly appreciated the support and mentorship that Prof. Garth Hobson and Dr. Anthony Gannon have provided during my time at the TPL. I have very much enjoyed being a part of the world-class research they conduct at this state-of-the-art facility. Their support, along with that of Milan Vukcevich, the Mechanical and Aerospace Engineering (MAE) network specialist, has allowed me to conduct the lengthy and resource-intensive computational fluid dynamics (CFD) simulations required to complete this thesis. Thanks are also in order to those students who have preceded me in their research on the Cross-Flow Fan (CFF). In particular, a big thank you is given to Christopher Delagrange for the models he had created that I was able to build upon, as well as to Ing Khang and BingQiang for their advice and assistance in the CFD simulations. Thank you also to the faculty and staff of the Department of Mechanical and Aerospace Engineering, who have been training me for this one year and have provided me with a good foundation in mechanical engineering. You have helped to enable me to be successful at the Naval Postgraduate School. Finally, a huge thank you is given to my dear wife, Yin Leng, for her encouragement through the many long days and nights that were spent working to complete my thesis and academic studies. Her steadfast commitment to me has allowed me to succeed at NPS and as an officer. Now, at the end of this process, I am anxious to close this chapter of life and to return home to continue my career as an Air Warfare Officer.

THIS PAGE INTENTIONALLY LEFT BLANK

I. INTRODUCTION

A. OVERVIEW

The need for a small personal air vehicle to offset the reliance on the automobile for passenger transport has fueled the research in lift and propulsion devices for personal vertical take-off and landing (VTOL) vehicles. Helicopters have traditionally offered the flexibility of VTOL applications, allowing for ingress and egress into a limited space where fixed-wing aircraft do not have access. The performance penalties for using helicopters as compared to fixed-wing aircraft have been low speed, limited range, and restricted operational ceiling. Lift-fan–powered fixed-wing aircraft trade hovering efficiency for the benefit of better cruise flight efficiency. Additionally, ducted lift fans have the advantage of shielding users and bystanders from the rotating blades and loud noises. The cross-flow fan (CFF) is a lifting and propulsion device that retains the advantages of both a fixed-wing aircraft and a ducted lift fan. There is no upper limit to the rotor length-to-diameter ratio of a CFF, allowing the device to be installed along the entire length of the wing or lifting device. Also, the CFF discharged vector can be easily rotated about the fan axis since the fan has no angular requirements, further allowing the capability of VTOL by thrust vectoring.

B. BACKGROUND

The CFF was patented over a century ago. Today, CFFs are commonly found in heating ventilation and cooling (HVAC) systems, air curtains designed to maintain a boundary between two atmospheres, and within computer servers to circulate the air in cooling the electronic components. Figure 1 illustrates an example of a commercial CFF used to circulate air in a departmental store.

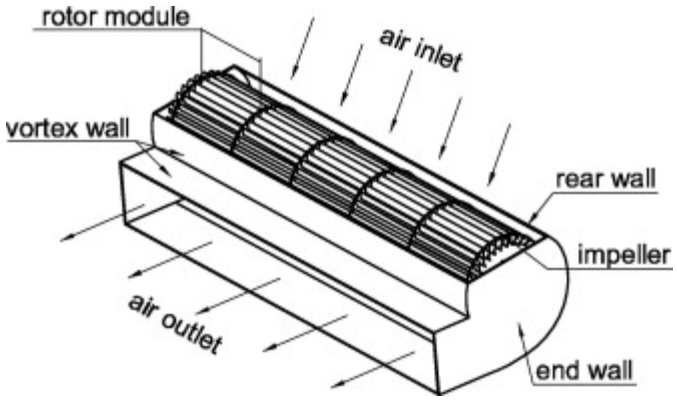

Figure 1. Commercial cross-flow fan (CFF)

Vought Systems Division (VSD) of the Ling-Temco-Vought (LTV) Aerospace Corporation was the first to explore using the CFF as a means of propulsion to augment concepts in the development of subsonic transport aircraft [1]. VSD conducted numerous studies and concluded that a CFF is capable of producing enough thrust to augment a heavy-lift aircraft's propulsion system.

In 2000, the researchers at the Naval Postgraduate School's Turbopropulsion Laboratory (TPL) sparked resurgence in the interest of CFF propulsion and conducted many CFF studies, such as:

- Gossett [2] proposed using a CFF to augment the vertical thrust of a single-seat VTOL aircraft.
- Cheng [3] performed an experimental and numerical analysis of a 12-inch diameter, 1.5-inch span CFF to validate VSD's research and develop a computational model of the CFF that could be further used for design modifications and improvements.
- Schreiber [4], Yu [5], and Ulvin [6] continued researching the performance of CFF rotors by modeling rotors of a smaller, 6-inch diameter over a range of spans from 1.5 inches to 6 inches to determine the CFF fan scaling laws.

- Cordero [7], as well as Gannon, Utschig, Hobson, and Platzer [8], incorporated the performance characteristics of a 6-inch diameter rotor with 30 double circular arc blades.
- Antoniadis [9] investigated altering the blade design and the number of blades on a CFF rotor to optimize its performance.

In 2006, Propulsive Wing, LLC successfully integrated a CFF into the trailing edge of an aircraft wing and demonstrated a Short Take-Off and Landing (STOL) flying model [10]. Although the current models produced by Propulsive Wing do not have the capability for VTOL, they are capable of performing near-vertical hovering when the plane is oriented at a steep angle of attack with the CFF operating. The company not only has developed an aircraft whose sole means of propulsion is powered by a CFF but also presented optimism to the future of a VTOL aircraft powered by CFF.

Most recently, Delagrange [11] analytically and experimentally modeled a CFF housing that resulted in a thrust-to-weight ratio of 0.616. CFFs possessed the potential to propel an airframe to flight; however adequate thrust must be produced by the CFF in order for it to realize VTOL. Most studies to date involve constructing CFFs with straight blades. Straight blades, however, produce noise levels that at high rotational speeds are unacceptable for personal air vehicle operation [12]. Hence, helical blades are believed to be able to solve the sound pressure level (dB) problem. Additionally, it is believed that helical blades could produce more thrust to aid in VTOL since helical blades transfer energy more efficiently from the rotor to the flow stream, allowing for faster rotational speeds of the rotor. This leads to the motivation to conduct a study to investigate the performance of a CFF with helical blades. This is the first time that such a study has been conducted. Hence, the results obtained with the helical-bladed model, will be compared with the experimental results obtained by Delagrange [11]. This thesis will specifically focus on computational fluid dynamic (CFD) modeling of CFF with helical blades.

C. OBJECTIVE

The main objective of this thesis was to investigate the performance of a CFF with helical blades in comparison to the CFF with straight blades. The helical-bladed CFF should reduce the sound pressure level as compared to straight-bladed CFF. Additionally, it was hoped that the performance (thrust) of the helical CFF would be comparable or better than that of the straight-bladed CFF.

D. SCOPE

The scope of the thesis is as follows:

- Construct both the straight- and helical-bladed CFFs using SOLIDWORKS.
- Run the simulations for both the models using ANSYS-WORKBENCH.
- Capture and analyze the results using CFD-POST.
- Conclude with the findings and make necessary recommendations.

II. DESCRIPTION OF THE ANALYTICAL MODEL

A. OVERVIEW

The previous study by Delagrange [11] treated the straight-bladed CFF simulation with CFD successfully. His modeled results were also close to the experimental results that he conducted. The experimental thrust measurements and analytically determined thrusts matched well over the entire CFF operating range, with a maximum error of 6.4% at the maximum operating speed of 8000 rpm [11]. In the case of power, for rotor speeds up to 6000 rpm, his ANSYS model accurately predicted the power. However, as the rotational velocity increased over 6000 rpm, the error between the measured and predicted powers grew extensively. The divergence between the predicted and actual powers was explained by the drop in CFF efficiency at speeds greater than 6000 rpm, as described by Anthoniadis [9] in his CFF performance research. Although Delagrange's model had straight blades, his experimental and analytical data was useful for comparing with the CFD results generated for the helical blades CFF (e.g., thrust and power generation).

The original CFF's full-size fluid model and its housing were created based on the following steps. Firstly, the rotor with straight/helical blades and the required housing were designed, created, and saved in PARASOLID format using SOLIDWORKS, a computer-aided drafting (CAD) program. Secondly, the models were exported to ANSYS-CFX to mate both the rotor and housing into a single model, following which the model was exported to the meshing tool for grid generation. Details of the mesh generation parameters were described in Appendix A. Thirdly, the generated mesh was imported into ANSYS-CFX-Pre to set up the appropriate boundary conditions and the solution parameters (see Appendix B for details). Once the changes in ANSYS-CFX-Pre were saved, a definition file (*.def) was created. This was the file required by the ANSYS-CFX-Solver to execute the simulation and generate the solution for the model. Lastly, the generated results for each simulation were processed in CFD-POST.

B. GEOMETRY AND GRID GENERATION

Initially, a 4-inch rotor with a greater turn (90°) helical blades was modeled. Details of this geometry were presented in Appendix C.

The geometric models of the CFF were created in SOLIDWORKS. The CFF model consisted of two major parts: the 8-inch rotor domain with 16 straight or helical blades, and the housing domain with the same length (as shown in Figures 2, 3, and 4). The helicity on the 8-inch rotor was limited to 10° over its length, as this was deemed to be the most realistic rotor that could be produced in the near term. The housing was designed by Delagrange [11].

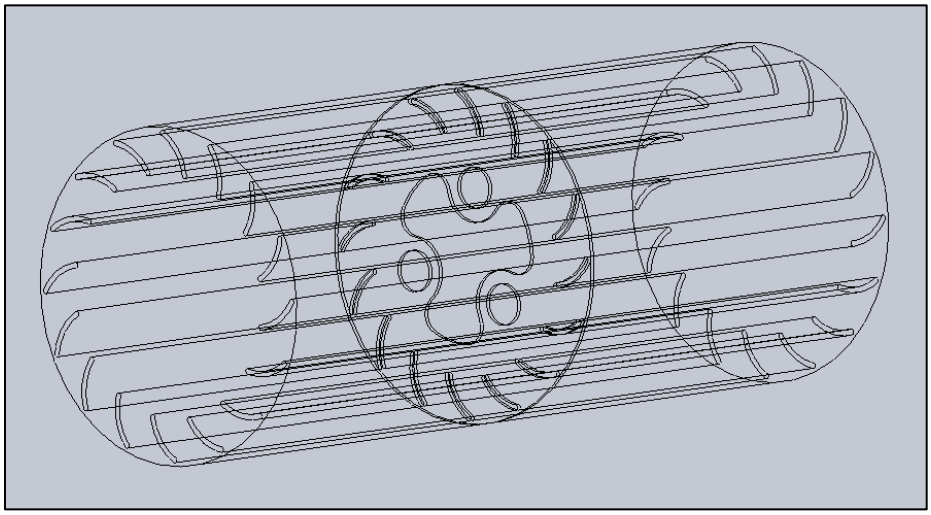

Figure 2. SOLIDWORKS model of an 8-inch CFF with 16 straight blades

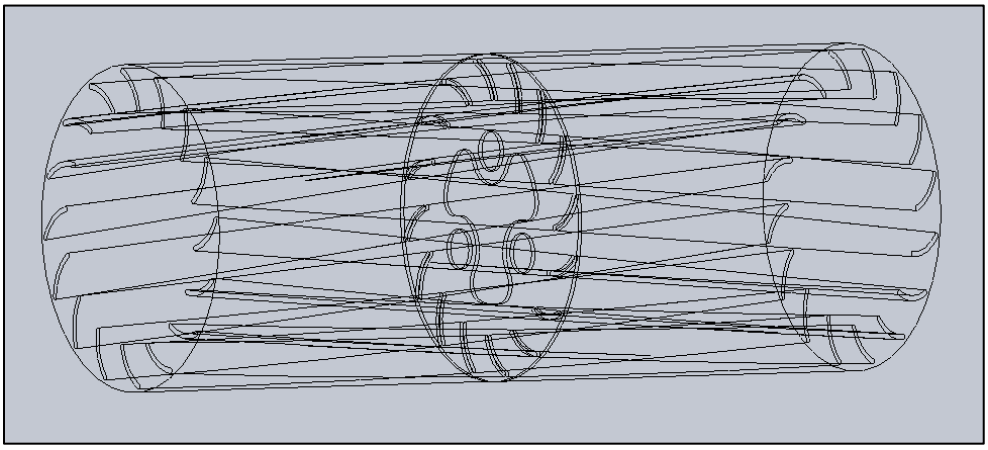

Figure 3. SOLIDWORKS model of an 8-inch CFF with 16 helical blades

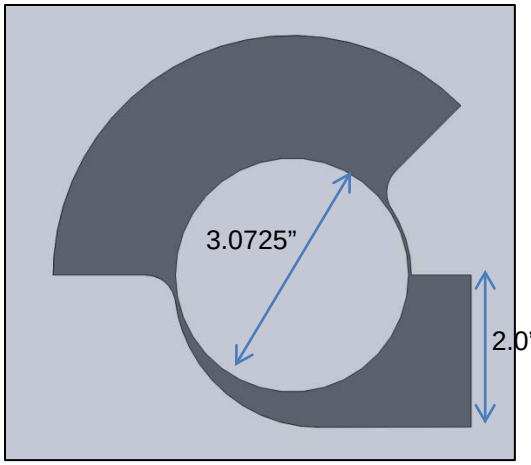

Figure 4. SOLIDWORKS model of a housing for the CFF

Because the models for the study were three-dimensional (3-D), they were created in the format of a fluid (as shown in Figure 5). Each model, in PARASOLID format, was imported into ANSYS-WORKBENCH to mate into a single model (as shown in Figures 6 and 7). The advantage of this strategy, mating in ANSYS-WORKBENCH DesignModeler instead of assembling in SOLIDWORKS, was to ensure that there would not be any irrelevant features or parameters created while combining the two models into one. In order to ensure that ANSYS-WORKBENCH recognized the model as two components, the material of the housing had to be chosen to be added as frozen. The model was then defined as a fluid domain and exported for grid generation.

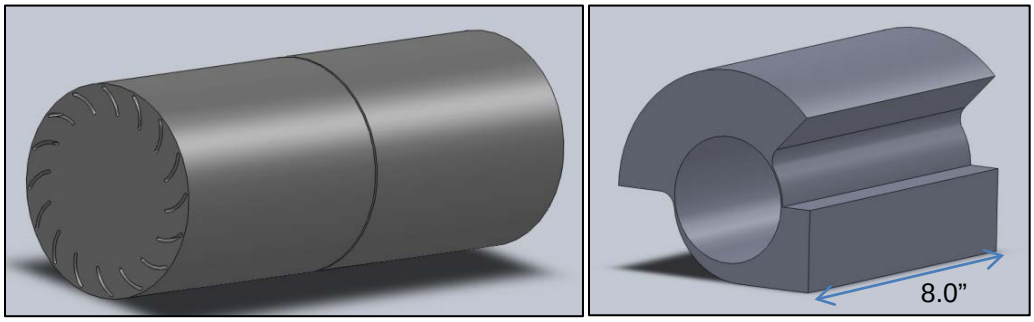

Figure 5. SOLIDWORKS model of rotor and housing domains illustrated in fluid format

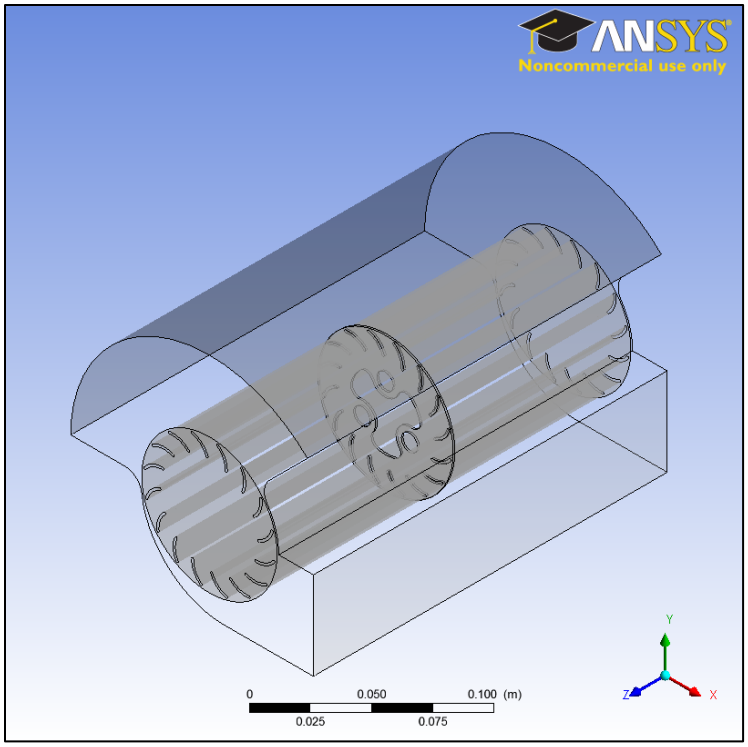

Figure 6. DesignModeler assembly of a straight-bladed CFF within its housing

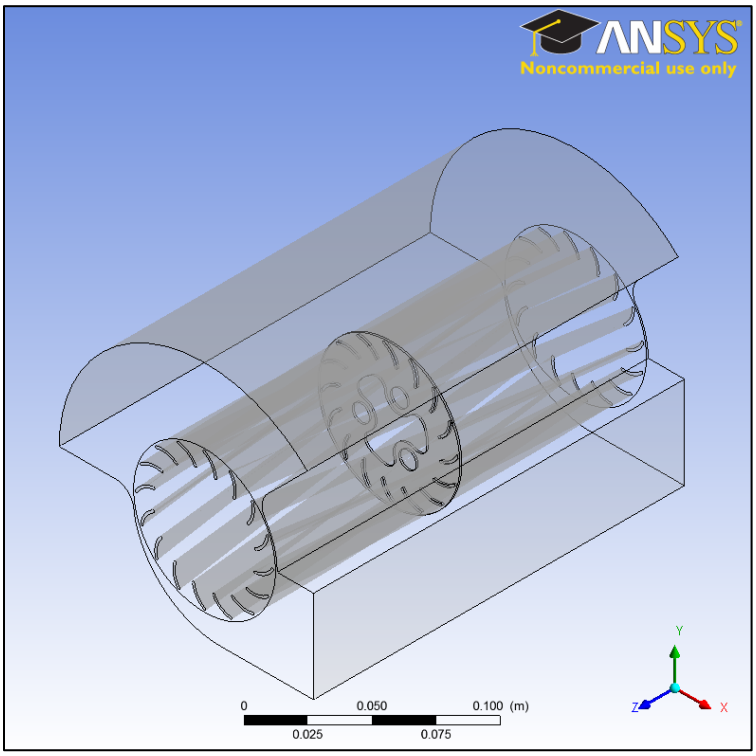

Figure 7. DesignModeler assembly of a helical-bladed CFF within its housing

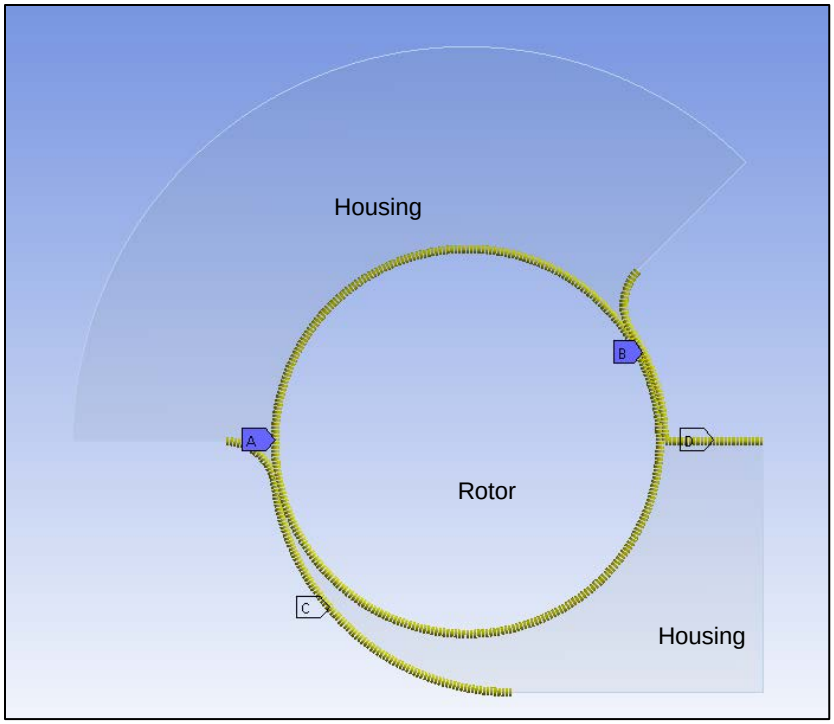

Figure 8. Locations where edge sizing were implemented

The models' mesh was generated within ANSYS-MESHER. In order to ensure that similar quality of meshes was generated in both the rotor and housing (for both straight- and helical-bladed models), edge sizing was implemented on both components, and the number of divisions for each side of the rotor and the housing (see Figure 8 and further details of illustration in Appendix A) were chosen as follows:

Table 1. Number of divisions for edge sizing on both rotor and housing

	Number of Divisions	
Sides	**Housing**	**Rotor**
A	310	310
B	45	-
C	110	-
D	25	-

The initial mesh for the 3-D CFD model of the straight-bladed CFF contained 4,655,488 nodes that were connected to form 23,913,666 elements. This coarse mesh was acceptable for the estimation of the airflow through the CFF for the study and was as shown in Figures 9 through 12.

Similar considerations were applied to the helical-bladed CFF in order to ensure a fair comparison between the two models.

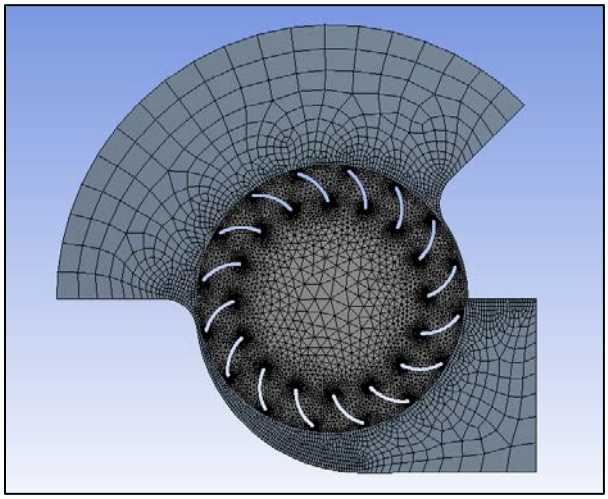

Figure 9. Mesh generated in the CFF assembly for the analysis (front view)

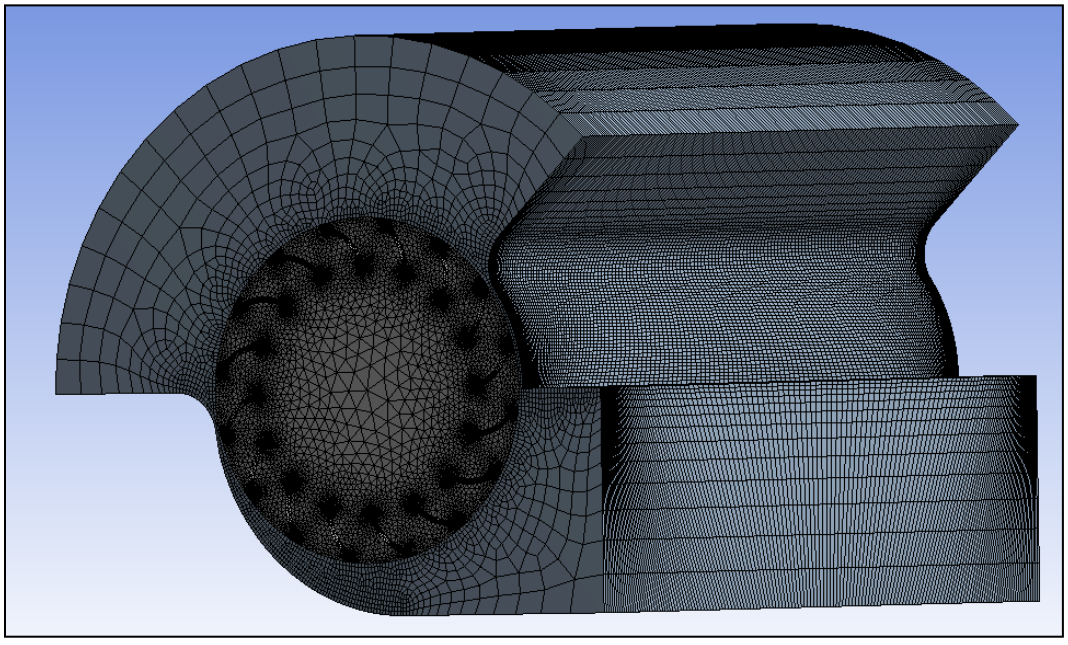

Figure 10. Mesh generated for the CFF assembly illustrated in 3-D

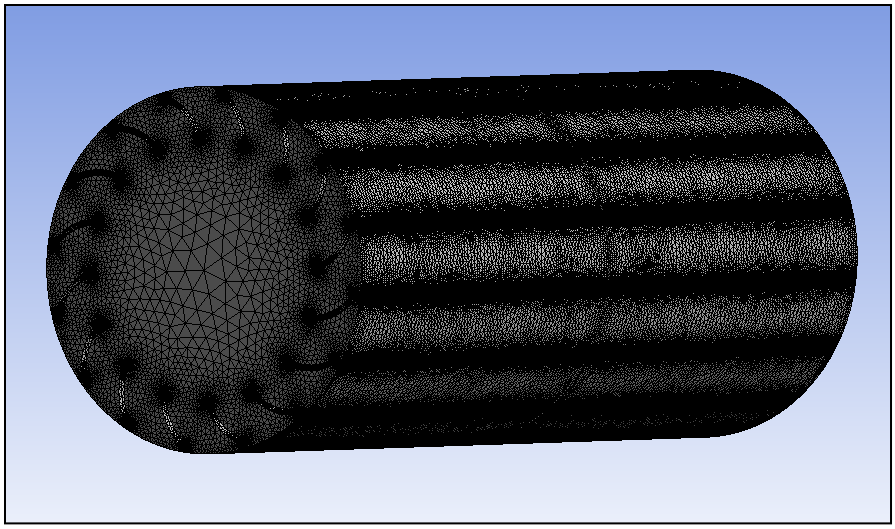

Figure 11. Mesh generated for the CFF rotor in 3-D

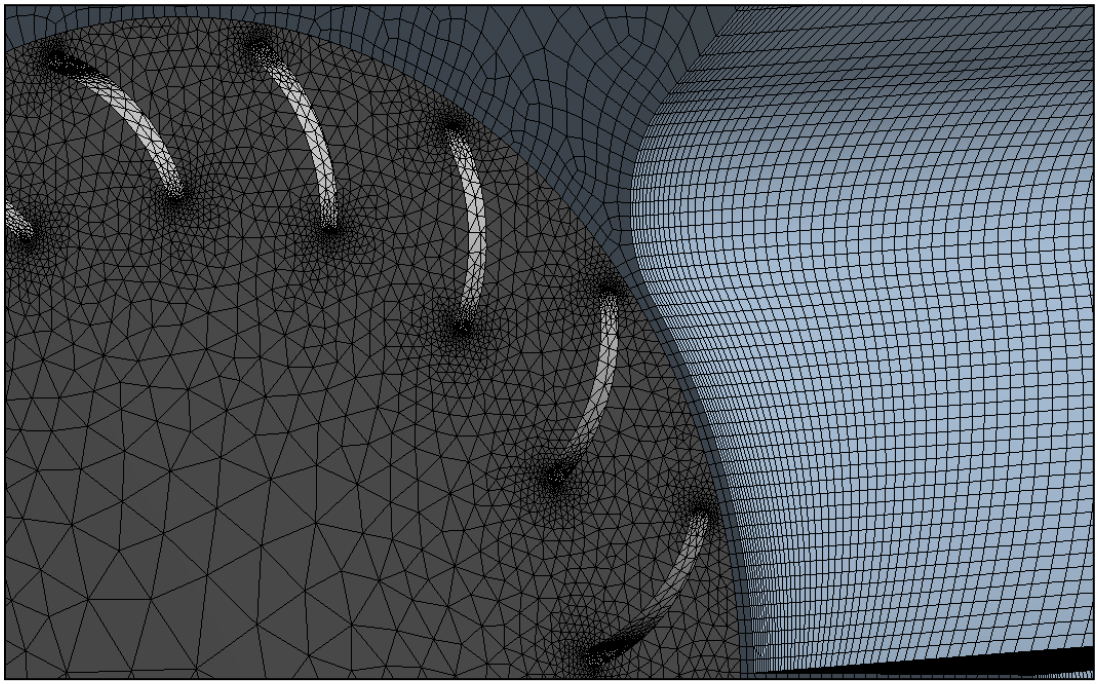

Figure 12. Detailed highlight of a section at the rotor domain and housing domain interface of the CFF

Table 2. CFF mesh assemblies' statistics

	Straight-Bladed CFF		Helical-Bladed CFF	
Mesh Type	Nodes	Elements	Nodes	Elements
Coarse	4,655,488	23,913,666	4,706,881	24,219,812
Fine	4,709,936	23,952,965	4,756,224	24,224,653

As listed in Table 2, the differences between the coarse and the fine meshes for both models were insignificant, given the large number of elements generated for the mesh. Due to the significantly large mesh elements, there was no intention to make use of the fine mesh or attempt to refine the mesh for the study, as the computation time for the coarse mesh was on the magnitude of 0.5 of a week per revolution. Besides being time-consuming to generate the mesh, the process of generating the mesh was also resource intensive. In order to reduce the time taken in generating the mesh, more resources in terms of high-computing-power computers with more processors as well as more ANSYS licenses were required. It was concluded that it would be excessively timely and computationally and resource expensive to perform the simulation runs if more elements were generated. Hence, it was deliberately decided that the CFD model with coarse mesh was a good enough model to meet the modeling requirements. While the method of mesh generation was significantly different than the mesh generated by Delagrange [11] during his analysis, the resulting mesh was assumed to be capable of producing results in an accurate representation of the experimental data when used in conjunction with the k-epsilon (k-ε) turbulence model.

C. METHODOLOGY AND BOUNDARY CONDITIONS

The CFF flow field was chosen to be transient, and not steady-state, since the rotor was in continuous rotation. Due to the transient nature of the simulation, the interface between the rotor and housing was selected as "Transient Rotor-

Stator" in ANSYS-CFX-Pre. Typically, the solver of the transient model needs the specification of some initial values by the user. These values could be omitted by selecting transient initialization override. The fluid was selected as air-ideal gas with constant specific heat at constant pressure. The reference pressure was set at one atmosphere. As shown in Figure 13, the inlet was specified as total pressure, while the outlet was specified as a free opening because an uncertainty existed with regard to the flow direction during the start of the simulation. The static temperatures at both the inlet and outlet were specified as 300K. The no-slip condition was selected for all the wall surfaces. The straight-bladed CFF rotor walls were specified as symmetry whereas helical-bladed CFF rotor walls were applied with free-slip condition.

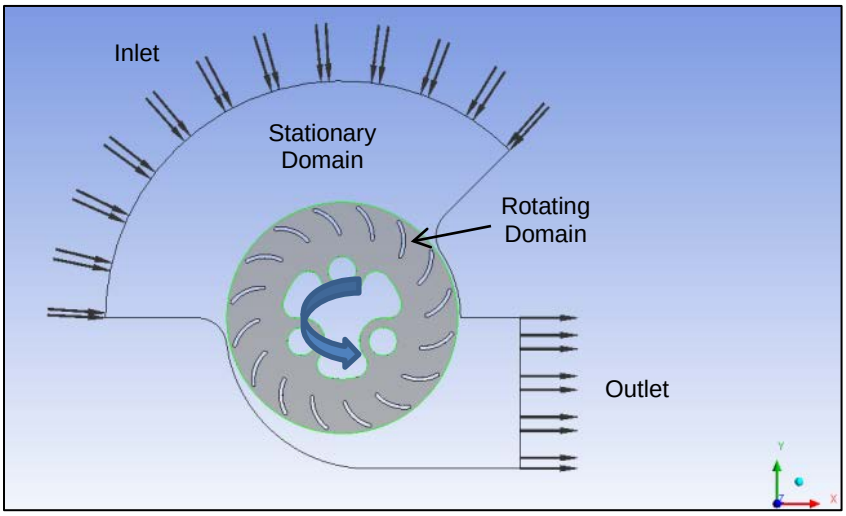

Figure 13. CFX-Pre model of a CFF within a housing (side view)

Two monitoring points were set for the simulation, one for measuring the rotor torque and the other for exit pressure. The torque was set by inputting an expression (torque()_z@Default Rotor). The purpose of this expression was to allow the user to monitor if the CFF had reached its stabilization point as well as to measure the torque, and power variations. As for the pressure, it was measured at a specific point within the CFF. In this case, the specific point was located at X: 0.058m, Y: -0.025m, Z: 0.1021m, which was located very near to

the middle span of the outlet (see Figures 14 and 15 for the yellow plus sign). The purpose was to monitor the pressure at this particular point at the outlet, so that the exit pressure could be compared to future experimental measurements of sound pressure levels.

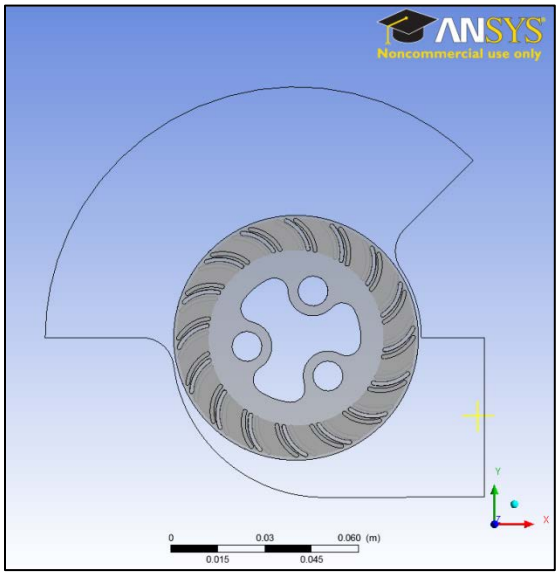

Figure 14. Pressure-monitoring point at the outlet (side and front view)

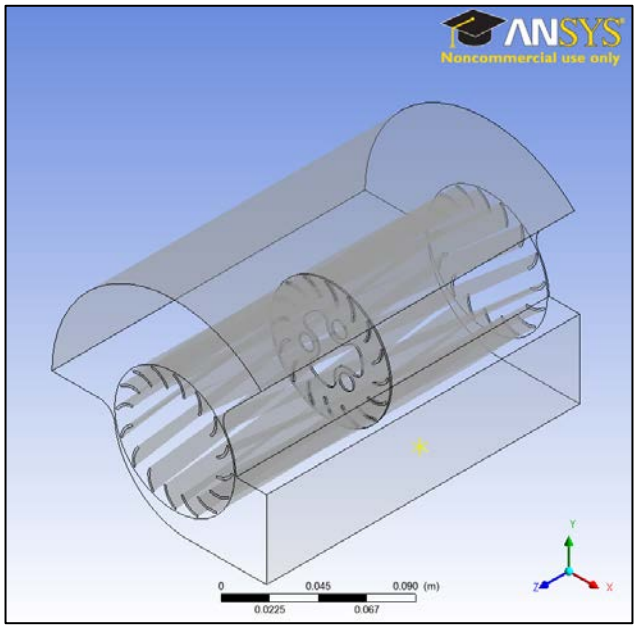

Figure 15. Pressure-monitoring point at the outlet (isometric view)

The center of rotation was the axis of the rotor, which coincided with the z-axis. Special care had to be given when defining the rotor speed to ensure the correct rotating direction (positive or negative, depending on the flow direction). The parameters for the total energy model and k-epsilon turbulence model were selected in order to include work input and turbulence phenomena. The automatic time-stepping method was used, which was similar to Antoniadis [9]. The following were the equations that the solver used, including continuity, momentum, energy, turbulence eddy dissipation, turbulent kinetic energy, and an equation of state:

Continuity Equation:

$$\frac{\partial \rho}{\partial t} + \nabla \bullet \left(\rho U\right) = 0 \tag{1}$$

Momentum Equation:

$$\frac{\partial \rho U}{\partial t} + \nabla \bullet \left(\rho U \otimes U\right) = \nabla \bullet \left(-p\delta + \mu\left(\nabla U + \left(\nabla U\right)^{T}\right)\right) \tag{2}$$

Energy Equation:

$$\frac{\partial \rho h_{tot}}{\partial t} - \frac{\partial \rho}{\partial t} + \nabla \bullet \left(\rho U h_{tot}\right) = \nabla \bullet \left(\mu \nabla T\right) + \nabla \bullet \left(\mu \nabla U + \nabla U^{T} - \frac{2}{3}\nabla \bullet U\delta U\right) \tag{3}$$

$$h_{tot}\left(p, T\right) = h_{stat}\left(p, T\right) + \frac{1}{2}U^{2} \tag{4}$$

Turbulent Eddy Viscosity:

$$\mu_{t} = C_{\mu}\rho\frac{k^{2}}{\varepsilon} \tag{5}$$

Turbulent Kinetic Energy:

$$\frac{\partial(\rho k)}{\partial t}+\nabla\bullet(\rho U k)=\nabla\bullet\left[\left(\mu+\frac{\mu_t}{\sigma_k}\right)\nabla k\right]+P_k-\rho\varepsilon \tag{6}$$

Turbulent Eddy Dissipation:

$$\frac{\partial(\rho\varepsilon)}{\partial t}+\nabla\bullet(\rho U\varepsilon)=\nabla\bullet\left[\left(\mu+\frac{\mu_t}{\sigma_\varepsilon}\right)\nabla\varepsilon\right]+\frac{\varepsilon}{k}(C_{\varepsilon 1}P_\kappa-C_{\varepsilon 2}\rho\varepsilon) \tag{7}$$

The Equation of State:

$$\rho(p,T)=\frac{p}{R_0 T} \tag{8}$$

D. SIMULATION PLAN

The CFD simulation plan was developed to predict the performance of the CFF with straight and helical blades. These were to determine whether the helical blades would contribute to the increase of the thrust and power when comparing the results of the two models. After successfully proving the prediction that helical blades would produce higher thrust and power, the next step was to construct 3-D CFF models to predict their performance. The CFD simulation plan was developed to predict the performance of the CFF with full 8-inch straight blades in 3-D over a range of speeds from 6000 to 8000 rpm. All of the simulations began with the same initial conditions at the inlet and outlet of 0 Pa total pressure at subsonic flow regime and opening pressure respectively. Additionally, the initial air velocities normal to each of these boundaries was set at 0 m/s to represent the initial conditions of a stationary VTOL aircraft prior to take-off. Each prospective CFF design was simulated to run for six revolutions (to ensure convergence of the rotor torque) at different speeds, and solved using CFX-SOLVER's RADIAL partitioning. The obtained results would be compared with those obtained experimentally by Delagrange [11]. If the simulated results were close to the experimental results, the simulation would advance to 8000

rpm. Once the simulated results were close to the experimental results, the modeling of the CFF with helical blades would be conducted to predict its performance. Similar parameters would be set as per those conducted for the CFF with straight blades, i.e., range of speeds from 6000 to 8000 rpm. The ANSYS-CFX settings are listed in Appendix B.

THIS PAGE INTENTIONALLY LEFT BLANK

III. BASELINE CFD MODEL RESULTS

A. MODEL VALIDATION

This was the first time the performance of a CFF with helical blades was investigated; thus, the approach taken was rather conservative. It was important to ensure that the CFF with helical blades could indeed increase the thrust and power before attempting the next step of increasing the sweep (helicity) of the blades.

The original carbon fiber CFF is of 8-inch length. Before attempting to model the complete version of the 8-inch rotor, a 4-inch rotor was constructed using SOLIDWORKS, and CFD analysis was performed to determine if the quarter turn helical blades did contribute to increasing the thrust and power. From the results gathered for both the 4-inch straight- and helical-bladed CFF, as shown in Figure 16 and Table 3, it was clearly observed that the helical blades did aid the CFF to produce more thrust and power as compared to the CFF with straight blades.

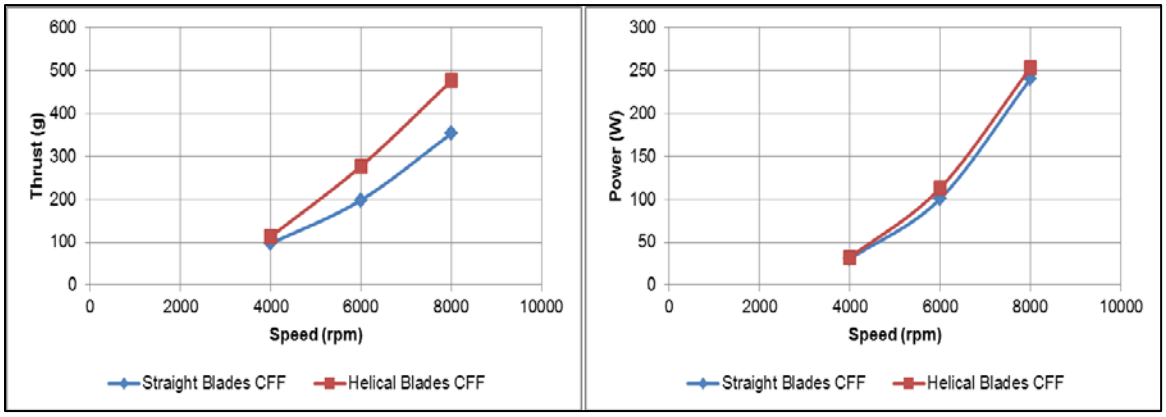

Figure 16. Comparison between 4-inch straight- and helical-bladed CFF

Table 3. Results for 4-inch straight- and helical-bladed CFF

S/N	Speed (RPM)	Straight		Helical	
		Thrust (g)	Power (W)	Thrust (g)	Power (W)
1	4000	96.854	30.4661	113.176	31.8893
2	6000	198.075	100.557	277.378	112.976
3	8000	353.343	240.371	476.452	253.03

1. 8-IN STRAIGHT-BLADED CFF MODELING

The successful completion of the analysis of the 4-inch CFF led to the modeling of a complete 8-inch CFF 3-D model. The 8-inch straight-bladed CFF models, together with the housing were constructed using SOLIDWORKS. In order to compare the CFD model with the experimental results obtained by Delagrange [11], the simulation had to replicate his experimental (straight blades) results as closely as possible. This was to ensure that the baseline (referring to the straight-bladed model) CFD model was able to achieve the same performances as in Delagrange's experiment before proceeding to model the 8-inch CFF with helical blades.

2. CONVERGENCE OF ANALYTICAL RESULTS

In Delagrange's [11] study of the two-dimensional (2-D) analytical model of the CFF, it was found that mass flow rate, total pressure ratio, total temperature ratio, and efficiency all converged to their steady state values after five revolutions of the model. This was also in accordance with the findings of Yu's [5] study. Using these previous findings as a precedence, the assumption was made that the 3-D model should converge after completing five revolutions. In this 3-D modeling study of the CFF, to determine the convergence of the state values, the rotor torque was analyzed over six revolutions. This approach was similar to the approach adopted by Delagrange [11]. The main difference was that an extra revolution was added as a conservative measure to ensure

convergence due to the complex nature of the 3-D simulation. As seen in Figure 17, the rotor torque was stabilized to a steady-state after six revolutions were completed.

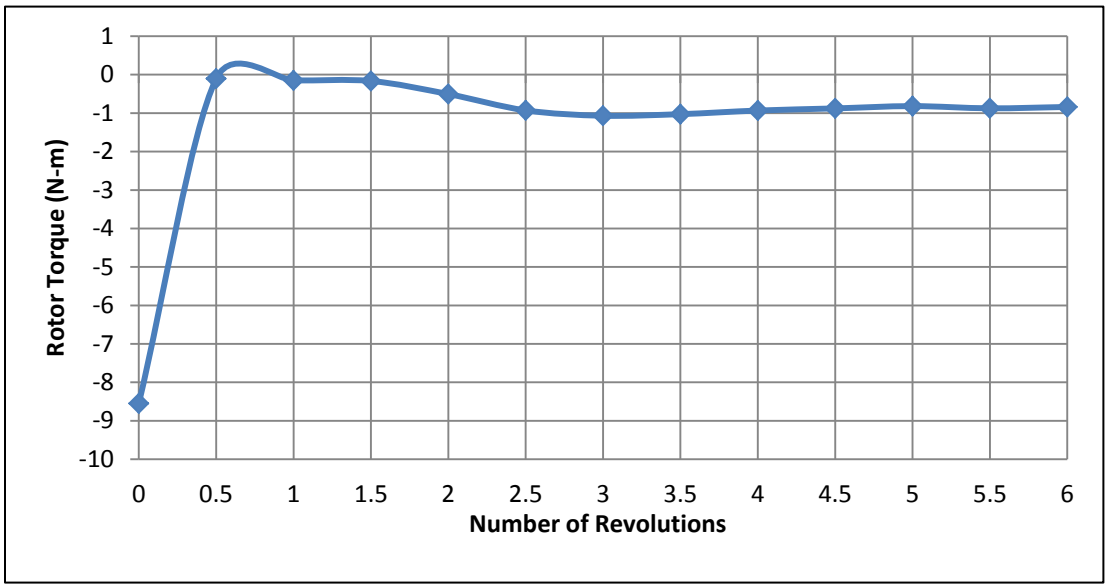

Figure 17. Convergence of rotor torque for 3-D straight-bladed CFF at 8000 rpm

3. RESULTS AND DISCUSSION

Table 4. Comparison of numerical and experimental results [From 11]

Speed (rpm)	Experimental Results [11]		3-D 8-inch Straight Blades CFD Results	
	Thrust (g)	Power (W)	Thrust (g)	Power (W)
6000	668.677	348.48	795.373	305.054
8000	1331.608	961.95	1371.469	703.333

As shown in Table 4, the results obtained from the CFD model for the straight-bladed CFF were quite close to the experimental results obtained by Delagrange [11]. In terms of the thrusts, the CFD results were very close to the experimental results as measured by Delagrange [11]. The powers that Delagrange [11] measured in his thesis were values required to drive the entire experimental set-up, which comprised components such as the motor and the

CFF rotor. This was the power consumption of the electric motor driving the CFF. The efficiency of the motor could possibly be deduced from the torque variations of the simulation. From the stabilized data, a snapshot (of a single revolution) of the torque's data from the 3-D CFD model was extracted (as shown in Figure 18). It was found out that the variations between the maximum and minimum torque were approximately 21.93%. Taking into consideration the power applied by Delagrange [11], this percentile would equate to a power of approximately 750.994W, whereby the CFD 3-D model's power was quite close.

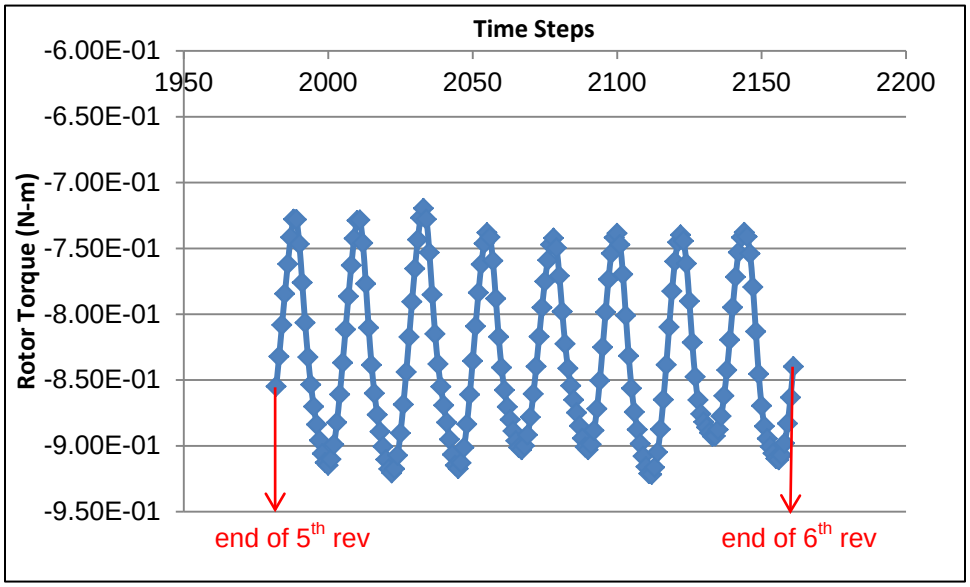

Figure 18. Graphical plot of the torque for 3-D CFF with straight blades model

From the contour plots of both the experimental and analytical results shown in Figures 19 and 20 respectively, it was observed that the velocity generated by both models were agreed very well. Both Delagrange's experimental and the 3-D analytical straight-bladed models output a velocity about 55 m/s.

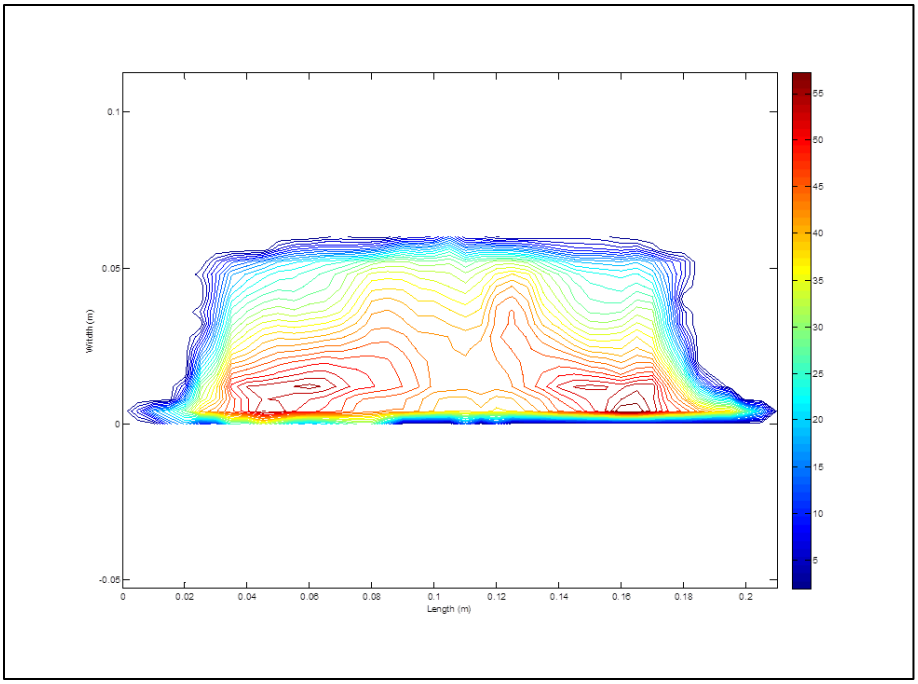

Figure 19. Experimental outlet velocity distribution (From [11])

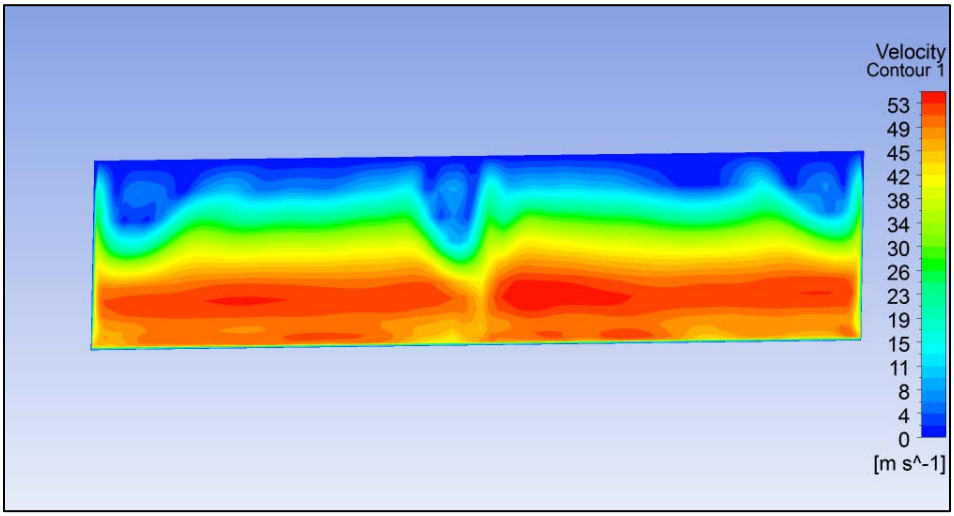

Figure 20. Predicted outlet velocity distribution

With the successful attempts in simulating the experimental results using a 3-D CFF with the straight-bladed CFD model, the investigation of the performance of the helical-bladed CFF was executed.

THIS PAGE INTENTIONALLY LEFT BLANK

IV. HELICAL-BLADED CFF SIMULATION AND COMPARISON WITH STRAIGHT-BLADED CFF

With the successful simulation of the straight-bladed CFF in ANSYS through a 3-D model, the focus was set to analyze the performance of the helical-bladed CFF. The same parameters were used except that the blades were changed to one-tenth helically turned blades. The findings on the performance of the helical-bladed CFF versus straight-bladed CFF are discussed in the following sections.

A. CONVERGENCE OF ANALYTICAL RESULTS

Similar to the 3-D straight-bladed CFF, the convergence of the rotor torque for the helical-bladed CFF was analyzed over six complete revolutions, and the same observation was made. As seen in Figure 21, the rotor torque for the helical-bladed CFF also stabilized to a steady state after six revolutions were completed.

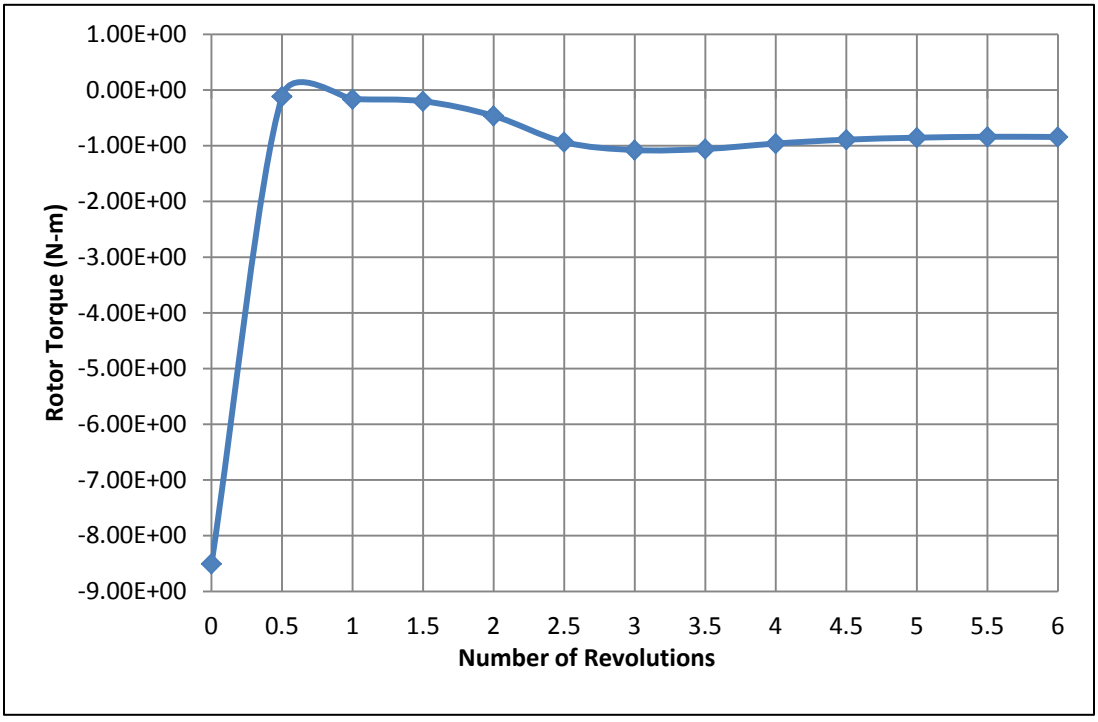

Figure 21. Convergence of rotor torque for 3-D straight-bladed CFF at 8000 rpm

B. FLOW VISUALIZATION

Figure 22 illustrated the flow through the CFF during the operation at speed of 8000 rpm. It could be observed that a vortex was formed both on the left and right side (circled in red in the figure) of the rotor. Similar observations were made by Delagrange [11] and Yu [5]. This vortex formation was expected and agreed with the observations in both [5] and [11], although the CFF in this case had helical blades.

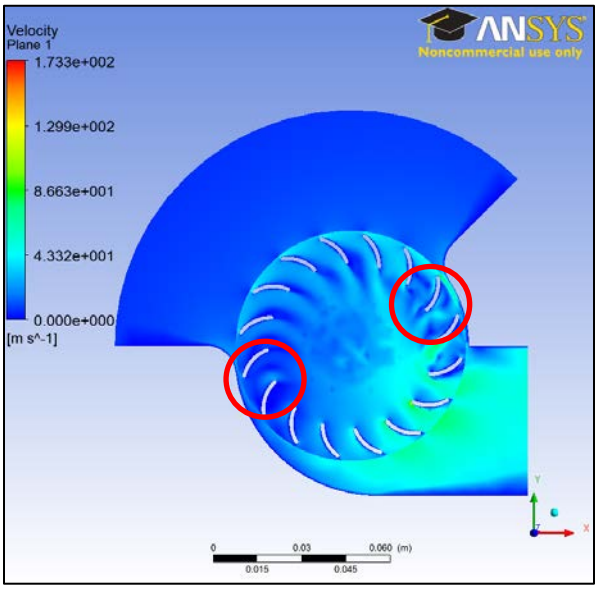

Figure 22. Air velocity through CFF at 8000 rpm

Figure 23 shows the velocity streamlines that were developed in the model at 8000 rpm. This figure illustrated that the CFF did not have stalled rotor blades across the entire inlet area surface. Similar observations were also made in Delagrange's experimental setup [11].

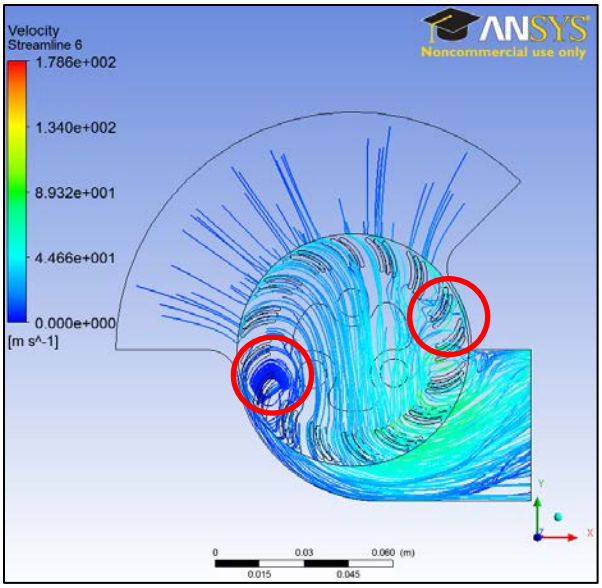

Figure 23. Air velocity streamlines in CFF at 8000 rpm

C. 3-D (HELICAL-BLADED) ANALYTICAL VERSUS EXPERIMENTAL (STRAIGHT-BLADED) RESULTS

The comparison between the 3-D helical-bladed CFF's analytical performance and Delagrange's [11] straight-bladed CFF experimental performance was made by comparing the generated thrust and the power. As highlighted by Delagrange [11], the comparison of the resulting velocities was the most crucial because both the thrust and the power were functions of the outlet velocity. Thus, the analytical formulation of the thrust and the power were calculated from the predicted outlet velocity as determined from CFD-POST after the completion of each run.

1. THRUST

Table 5 listed the compiled results obtained from ANSYS for the helical-bladed CFF, and they were compared with the straight-bladed CFF experimental results obtained by Delagrange [11] as well as the 3-D straight-bladed CFF analytical results.

Table 5. Comparison of numerical and experimental thrust results [From 11]

Speed (rpm)	Delagrange's experimental thrust (g) results [11]	3-D analytical straight-bladed CFF thrust (g)	3-D analytical helical-bladed CFF thrust (g)
6000	645.0000	795.3733	822.7510
8000	1161.0000	1371.4693	1488.7951

The thrust results were determined based on the outlet velocity and mass flow rate as obtained from the ANSYS CFX solutions. As observed from Table 5, the one-tenth turn on the CFF blades did contribute to an increase in thrust as compared to both the analytical and experimental results of the straight-bladed CFF. At 6000 rpm and 8000 rpm, comparing to the analytical 3-D straight-bladed CFF results, the increase in thrust generated by an one-tenth turn helical-bladed CFF was about 3.44% and 8.55% respectively. Figure 24 illustrated the increased thrust generated by the helical-bladed CFF in comparison to both Delagrange's experimental thrust measurements [11] and the analytical results.

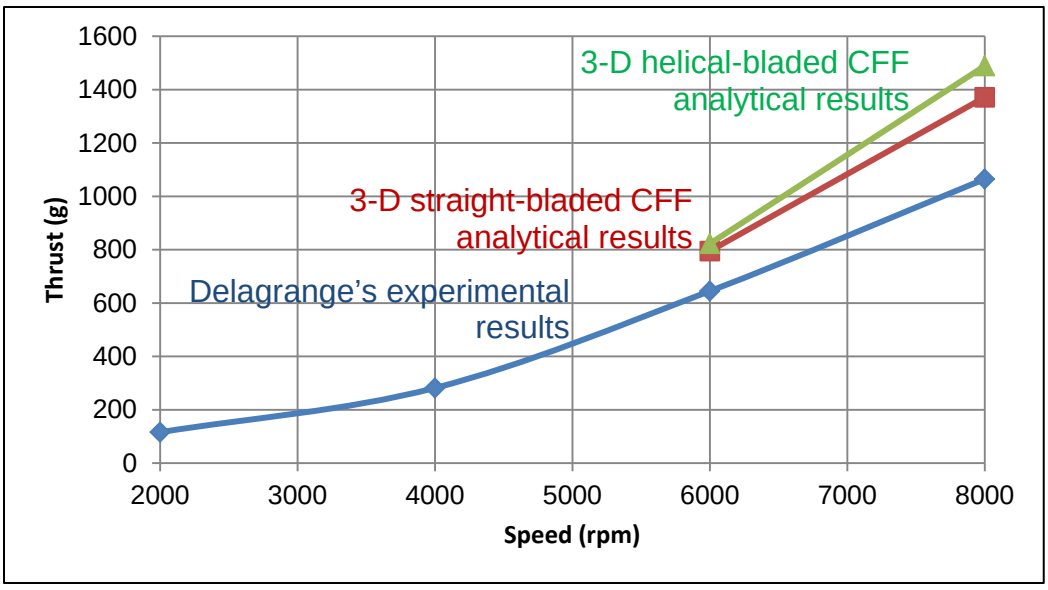

Figure 24. Graphical plot of numerical and experimental thrust results [From 11]

Taking the torque into consideration and compared between both the 3-D straight- and helical-bladed CFFs, the variations in torque for the case of the helical-bladed CFF were observed to be lower. See Figures 25 and 26 for the

comparison of the torque between the two rotors, and Figure 27 for a blown-up view for the helical blades CFF's torque variations.

This was a good phenomenon for the CFF because the lower the torque variations, the higher the efficiency of the rotor, which in turn produces more thrust.

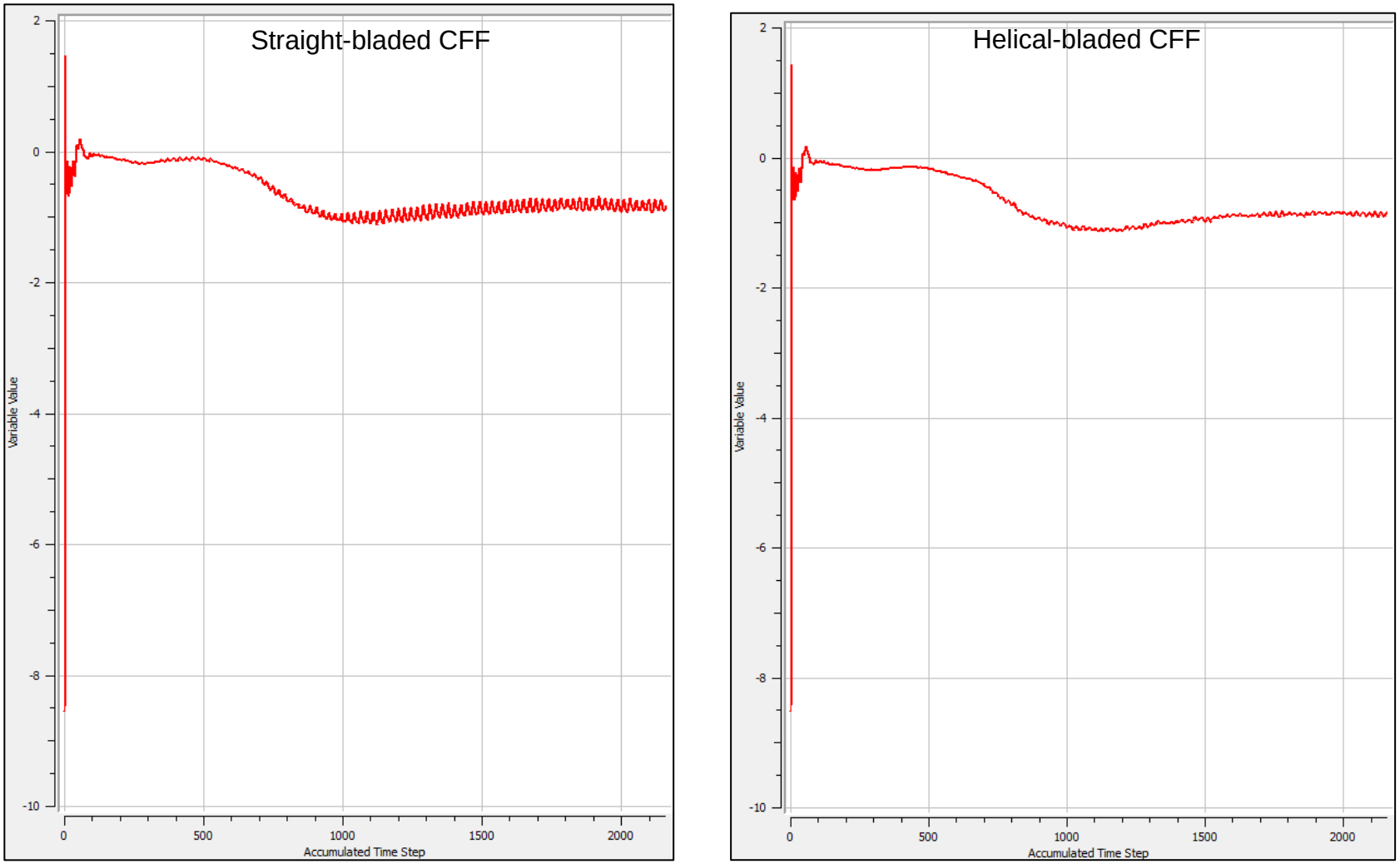

Figure 25. Comparing torque variations observed in both straight- and helical-bladed CFF

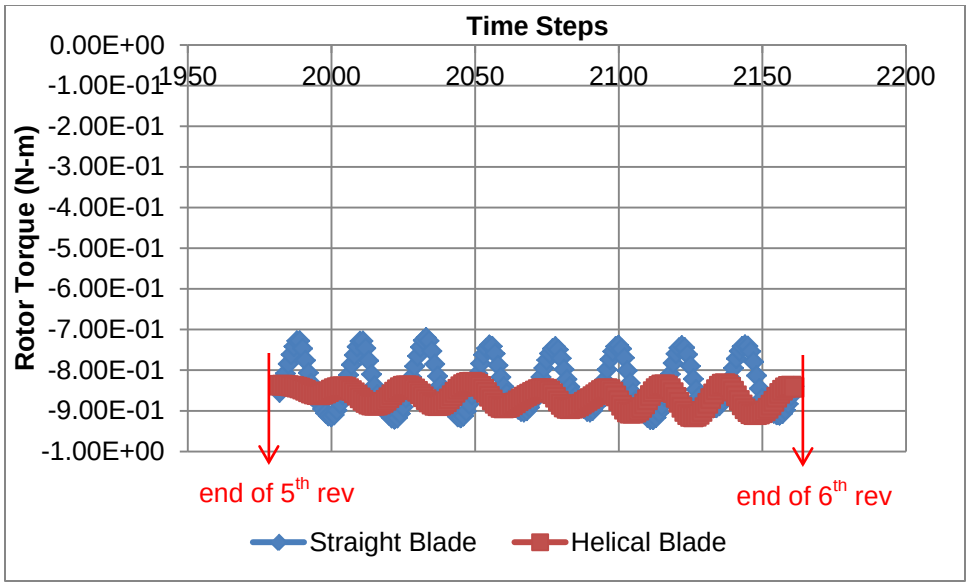

Figure 26. Rotor torque comparison between helical and straight blades models at 6th revolution

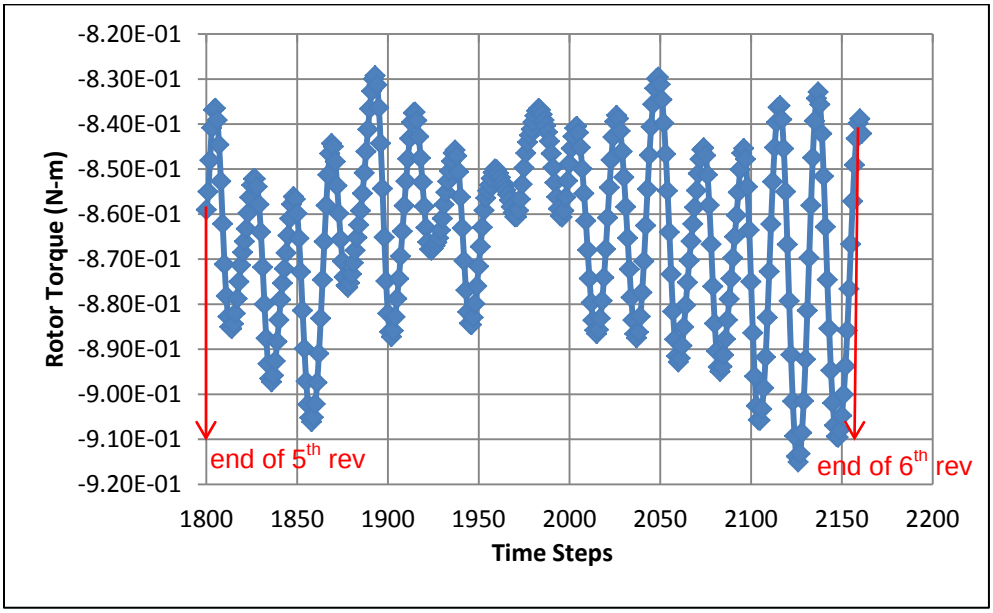

Figure 27. Blown-up view for the torque of 3-D CFF with helical blades model at 6th revolution

2. POWER

As described above, the helical-bladed CFF did contribute to increasing the thrust. Power was directly related to the thrust. Hence, the increase in thrust would lead to an increase in power absorbed. Table 6 showed the experimental power consumptions for the straight-bladed CFF and analytically determined power results for the straight- and helical-bladed CFF. As observed from the numbers in Table 6, with one-tenth helically turned blades, the CFF would generate 5.17% and 11.2% increase in power consumption as compared to the analytical straight-bladed CFF at 6000 rpm and 8000 rpm respectively. The discrepancy in power as observed between the experimental and analytical results for the straight-bladed CFFs was due to the fact that Delagrange [11] measured the power consumption of the electric motor driving the CFF. This experienced significant heat losses as the motor overheated during a run. Additionally, this could be due to the calculation done within CFD-POST. CFD-POST retrieved results from the last iteration of each completed run to conduct any calculation. Calculation done in this way could be inaccurate as the parameters were based on the last iteration and not based on an average over the entire run.

Table 6. Comparison of numerical and experimental power results [From 11]

Speed (rpm)	Delagrange's experimental power (W) results (see Appendix D)	3-D analytical straight-bladed CFF power (W) results	3-D analytical helical-bladed CFF power (W) results
6000	212.557	230.6710	242.6005
8000	597.3308	532.9497	592.6698

3. SOUND PRESSURE

The analytically determined CFF sound pressure level at the outlet could be seen in Figures 28 and 29. The analytical results were obtained by inserting a monitoring point at the outlet. These figures illustrated the sound pressure level

for 8000 rpm. As observed from the figures, the sound pressure level produced by the helical blades CFF was lower than the straight blades CFF, and was lowered by 6dB (calculated in terms of RMS value). This observation showed that the CFF with helical blades could potentially solve the sound level problem, which was inherently noisy with the straight-bladed CFF.

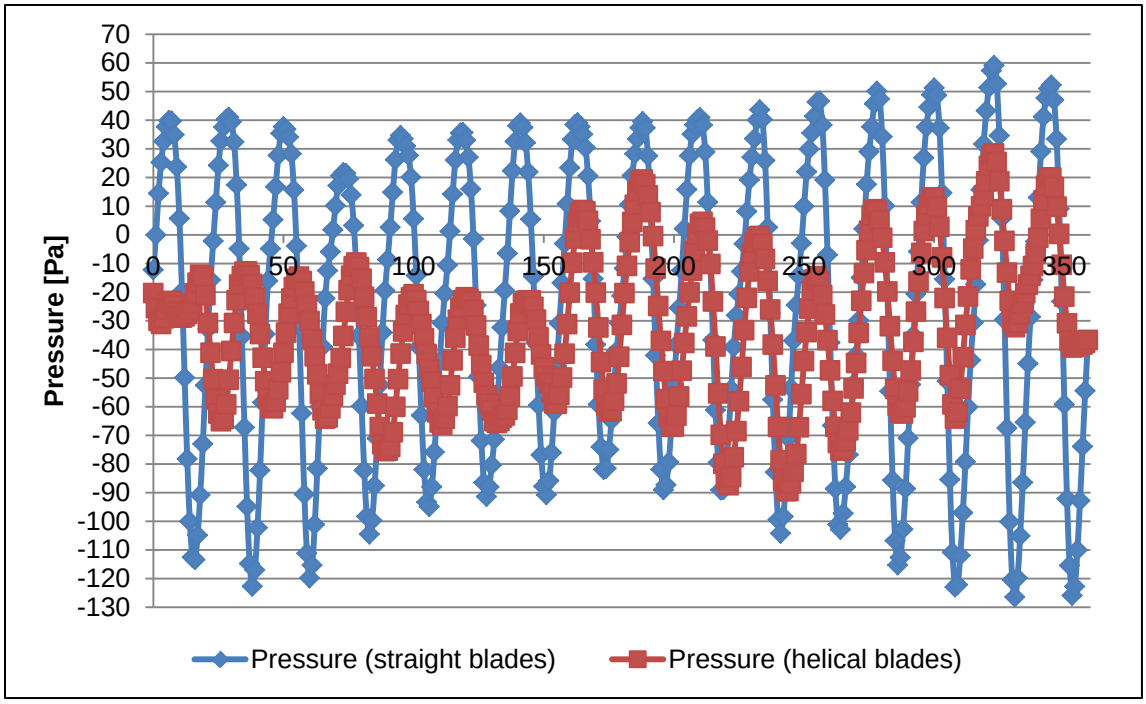

Figure 28. Comparison of analytical pressure results at the CFF outlet

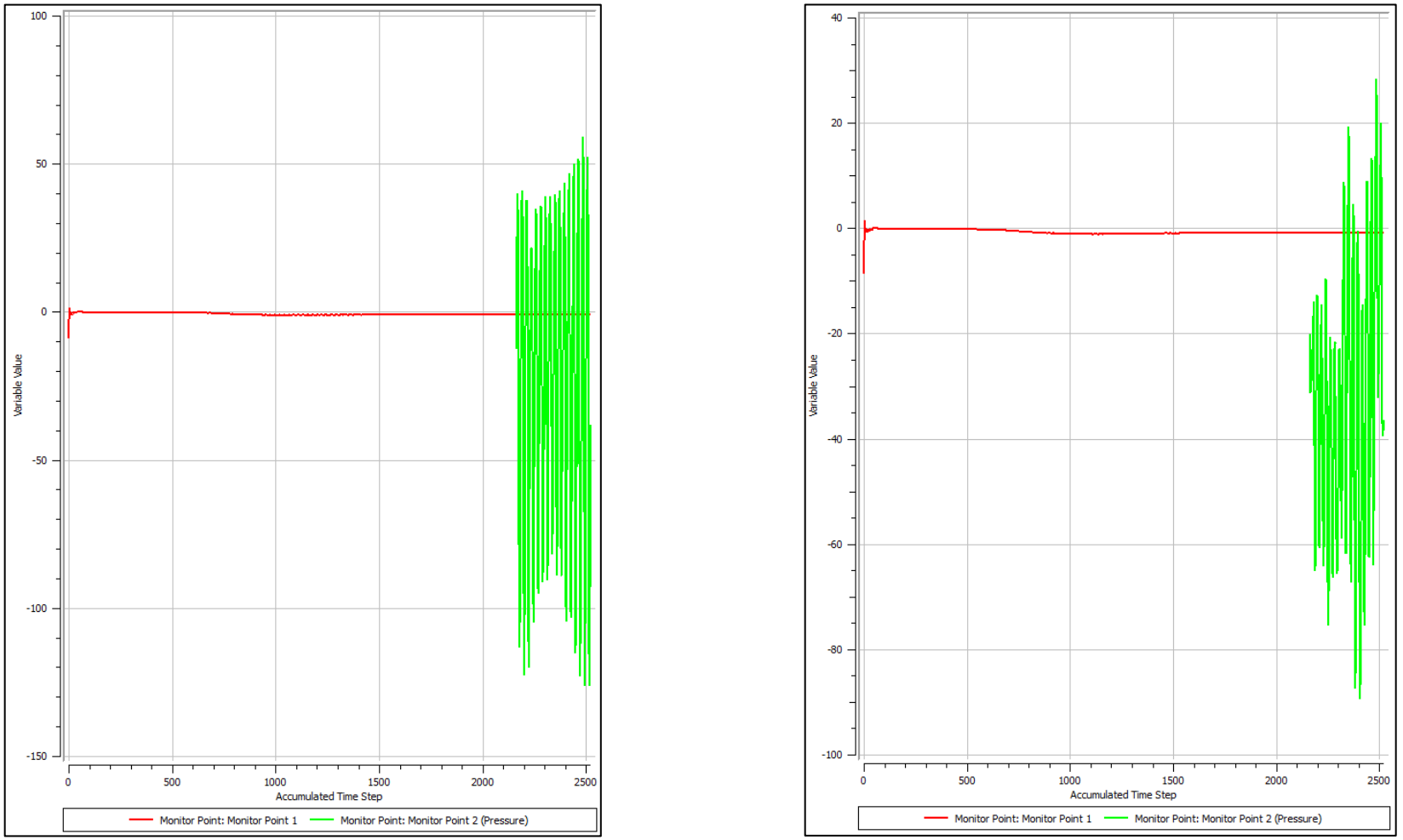

Figure 29. Sound pressure level comparison between straight-bladed CFF (left) and helical-bladed CFF (right)

V. CONCLUSIONS AND RECOMMENDATIONS

A. CONCLUSIONS

It was concluded that the CFF with helical blades could increase thrust production over straight-bladed CFF, and the produced thrust was optimistic to realize VTOL.

The propulsion system of a VTOL aircraft required maximum thrust during take-off and landing. Hence, the CFF would need to operate at its highest speed in order to generate the maximum thrust. As the VTOL aircraft transitioned to level flight, the CFF fan speed could be reduced to operate more efficiently during cruise. The maximum speed of operation of the helical-bladed CFF for this study was 8000 rpm, which resulted in a generated thrust of approximately 1488.7951 g.

As described by Delagrange [11], based on his initial configuration of the assembly the total weight for the above assembly weighed about 1729 g. His setup was able to provide sufficient power for his CFF operation. However, due to the laden weight, the thrust-to-weight ratio was reduced to 0.616. In the helical blades CFF case, basing on Delagrange's setup [11], the thrust-to-weight ratio was 0.861. Though the resulted thrust-to-weight ratio was also less than 1, it had increased with the aid of the helical blades. This was an optimistic observation as it had shown that helical blades CFF could generate more thrust and improve the thrust-to-weight ratio.

B. RECOMMENDATIONS

Moving forward, to carry on the investigation of increasing the thrust by the helical blades CFF, the following are some recommended area of studies.

Though expensive in terms of time and computations to run a simulation with a large number of mesh elements, it is recommended that generation of fine

mesh for the model should be explored to enable the determination of a more accurate fluid flow investigation.

In this study, the degree of twist applied to the helical blades of the CFF was one-tenth of a turn. A sensitivity study on the performance of helical-bladed CFF should be conducted to determine the relationship between the degree of turn and the performance of the CFF. This would determine the optimum amount of turning required to produce the desired thrust and power of a helical-bladed CFF. That understanding would, in turn, enable the researcher to know the requirements of the CFF before manufacturing and carrying out the actual experiment.

The Turbopropulsion Laboratory currently possesses the capability to build its own CFF straight-bladed rotors. With this capability, the Turbopropulsion Laboratory could build its own CFF helical-bladed rotors with various amounts of turning and different number of blades, and conduct experiments to investigate the performance of the helical-bladed CFF.

To realize VTOL, adequate thrust is required. Besides having helical blades to increase the thrust produced by the CFF, the CFF would also need to be driven to higher speeds to increase the thrust. Experimental runs could be conducted to investigate the amount of thrust a helical-bladed CFF will produce at higher speeds. The experiments would also be able to determine the highest speed a CFF with helical blades could operate.

In future, experimental studies could be conducted to measure the sound pressure level at the outlet of the rotor assembly by inserting a measuring probe at the outlet.

APPENDIX A. GENERATING MESH: EDGE SIZING

A. DESCRIPTION

Meshing was part of the modeling process to enable the communication of the model's geometry to the flow solver. Within the model, nodes were created and connected with elements, which allowed the communicating process for the simulation to take place. For the CFF, as the rotor was rotating while the housing was stationary, the edges within them around the housing and the rotor (as labeled in Figure 8) would need to take an extra step to ensure that the elements created were of similar sizing. This step was to enable smoother communication between the two components when the fluid was flowing through them. Hence, edge sizing was chosen.

B. SIZING PARAMETERS AND ILLUSTRATION

The edge sizing parameters required for the model were illustrated as follows:

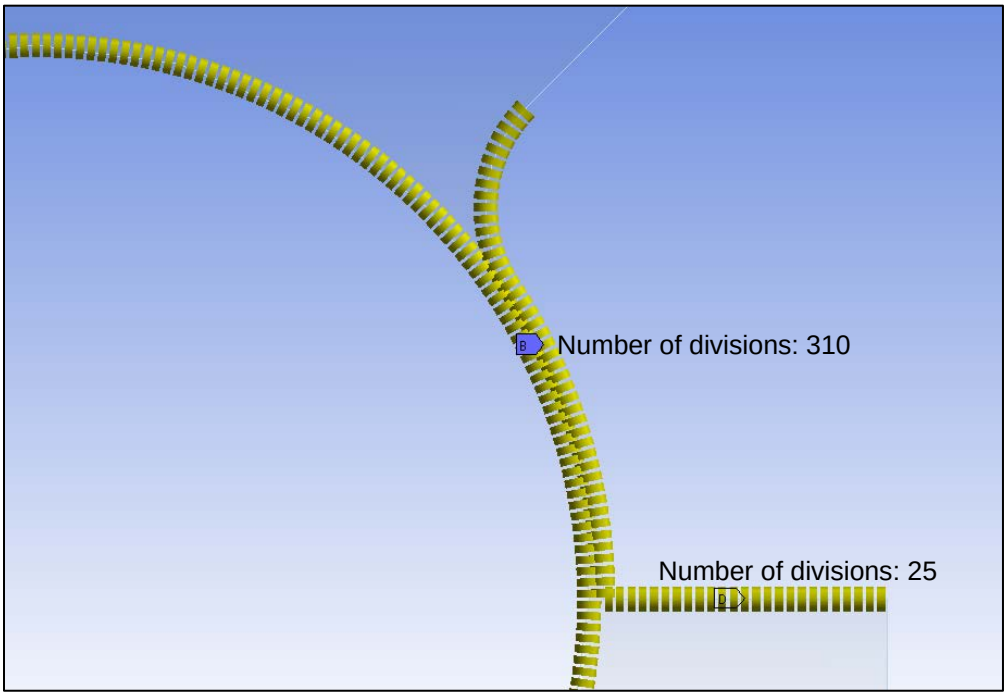

Figure 30. Blown-up view 1

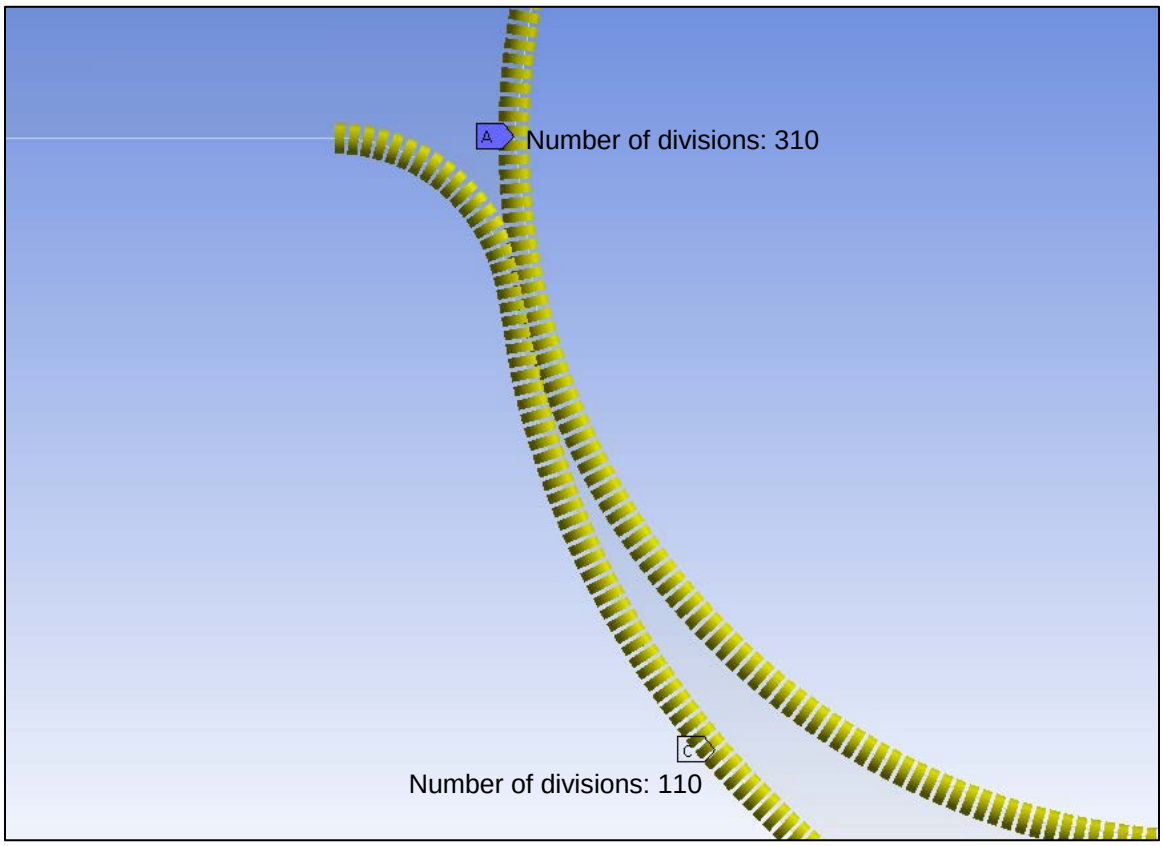

Figure 31. Blown-up view 2

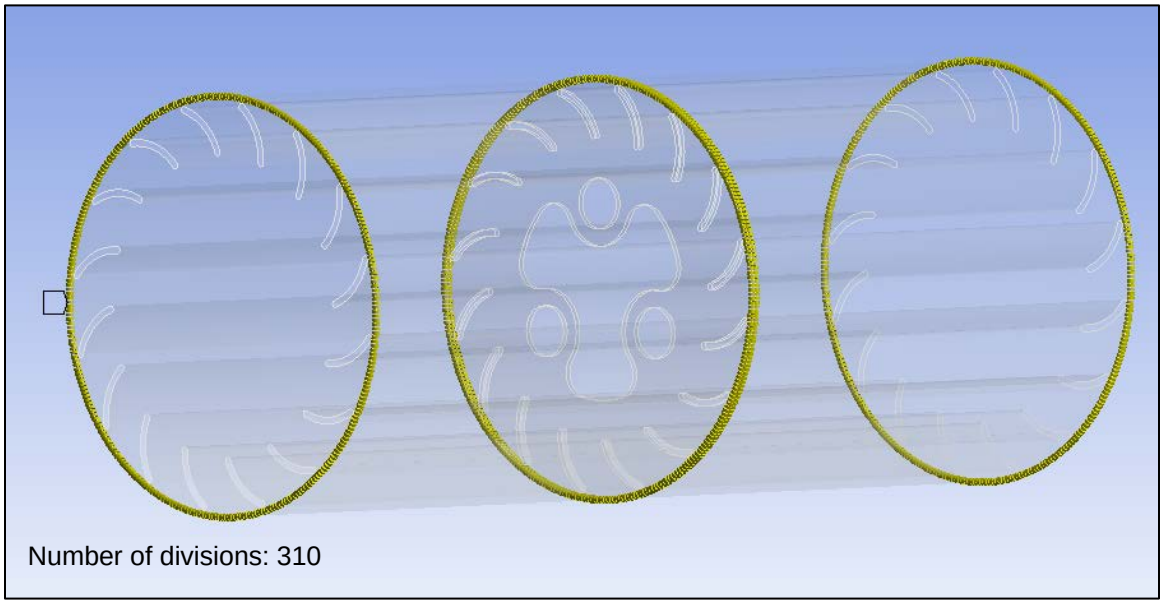

Figure 32. Applying edge sizing on the housing

APPENDIX B. ANSYS CFX PARAMETERS AT 6000/8000 RPM

Analysis Type	Basic Settings • External Solver Coupling o Option: None • Analysis Type o Option: Transient • Time Duration o Option: Total Time o Total Time: 0.06 / 0.045 [s] • Time Steps o Option: Time steps o Time steps: 2.7778e-005 / 2.0833e-005 [s] • Initial Time o Option: Automatic with Value o Time: 0 [s]
Rotor	Basic Settings • Location & Type o Location: B305 o Domain Type: Fluid Domain o Coordinate Frame: Coord 0 • Fluid and Particle Definitions o Fluid 1 ▪ Option: Material Library ▪ Material: Air Ideal Gas ▪ Morphology • Option: Continuous Fluid ▪ Minimum Volume Fraction: Unchecked • Domain Models o Pressure ▪ Reference Pressure: 1 [atm] o Buoyancy Model ▪ Option: Non Buoyant o Domain Motion ▪ Option: Rotating ▪ Angular Velocity 8000 [rev min^-1] o Axis Definition ▪ Option: Coordinate Axis ▪ Rotation Axis: Global Z o Mesh Deformation ▪ Option: None Fluid Models • Heat Transfer o Option: Total Energy o Incl. Viscous Work Term: Unchecked • Turbulence o Option: k-Epsilon o Wall Function: Scalable o High Speed (compressible): Unchecked o Turbulent Flux Closure for HT: Unchecked • Combustion o Option: None

	• Thermal Radiation o Option: None • Electromagnetic Model: Unchecked Initialization • Domain Initialization o Frame Type: Rotating o Coord Frame: Unchecked • Initial Conditions o Velocity Type: Cylindrical o Cartesian Velocity Components ▪ Option: Automatic with Value ▪ X Component: 0 [m s^-1] ▪ Y Component: 0 [m s^-1] ▪ Z Component: 0 [m s^-1] • Static Pressure o Option: Automatic with Value o Relative Pressure: 1 [Pa] • Temperature o Option: Automatic with Value o Temperature: 300 [K] • Turbulence o Option: Medium (Intensity = 5%)	
Rotor	Rotor Default	Basic Settings • Boundary Type: Wall o Location: (automatically fills out) o Coord Frame: Unchecked o Frame Type: Rotating Boundary Details • Mass and Momentum o Option: Free-Slip Wall o Wall Velocity: Unchecked • Wall Roughness o Option: Smooth Wall • Heat Transfer o Option: Adiabatic Sources • Boundary Source: Unchecked
Rotor	Symmetry	Basic Settings • Boundary Type: Symmetry • Location: RototSym1 RotorSym2
Housing	Basic Settings • Location & Type o Location: B665 o Domain Type: Fluid Domain o Coordinate Frame: Coord 0 • Fluid and Particle Definitions… o Fluid 1 ▪ Option: Material Library ▪ Material: Air Ideal Gas ▪ Morphology	

	• Option: Continuous Fluid ▪ Minimum Volume Fraction: Unchecked • Domain Models o Pressure ▪ Reference Pressure: 1 [atm] o Buoyancy Model ▪ Option: Non Buoyant o Domain Motion ▪ Option: Stationary o Mesh Deformation ▪ Option: None Fluid Models • Heat Transfer o Option: Total Energy o Incl. Viscous Work Term: Checked • Turbulence o Option: k-Epsilon o Wall Function: Scalable o High Speed (compressible): Unchecked o Turbulent Flux Closure for HT: Unchecked • Combustion o Option: None • Thermal Radiation o Option: None • Electromagnetic Model: Unchecked Initialization • Domain Initialization: Checked o Coord Frame: Unchecked • Initial Conditions o Velocity Type: Cylindrical o Cylindrical Velocity Components ▪ Option: Automatic with Value ▪ Axial Component: 0 [m s^-1] ▪ Radial Component: 0 [m s^-1] ▪ Theta Component: 0 [m s^-1] o Velocity Scale: Unchecked • Static Pressure o Option: Automatic with Value o Relative Pressure: 1 [Pa] • Temperature o Option: Automatic with Value o Temperature: 288.15 [K] • Turbulence o Option: Medium (Intensity = 5%)	
Housing	Housing Default	Basic Settings • Boundary Type: Wall o Location: (automatically fills out) o Coord Frame: Unchecked Boundary Details • Mass and Momentum o Option: No-Slip Wall o Wall Velocity: Unchecked • Wall Roughness

		○ Option: Smooth Wall • Heat Transfer ○ Option: Adiabatic Sources • Boundary Source: Unchecked
Housing	Inlet	Basic Settings • Boundary Type: Inlet • Location Inlet • Coord Frame: Unchecked Boundary Details • Flow Regime ○ Option: Subsonic • Mass and Momentum ○ Option: Total Pressure (stable) ○ Relative Pressure: 0 [Pa] • Flow Direction ○ Option: Normal to BC • Turbulence ○ Option: Medium (Intensity = 5%) • Heat Transfer ○ Option: Static Temperature ○ Static Temperature: 300 [K] Sources • Boundary Source: Unchecked Plot Options • Boundary Contour: Unchecked
Housing	Outlet	Basic Settings • Boundary Type: Opening • Location Outlet • Coord Frame: Unchecked Boundary Details • Flow Regime ○ Option: Subsonic • Mass And Momentum ○ Option: Opening Pres. And Dirn ○ Relative Pressure: 0 [Pa] • Flow Direction ○ Option: Normal to BC • Turbulence ○ Option: Medium (Intensity = 5%) • Heat Transfer ○ Option: Opening Temperature ○ Opening Temperature: 300 [K] Sources • Boundary Source: Unchecked Plot Options • Boundary Contour: Unchecked
Housing	Symmetry	Basic Settings

		• Boundary Type: Symmetry • Location: HousingSym1 HousingSym2
Interfaces	Housing to Rotor	Basic Settings • Interface Type: Fluid Fluid • Interface Side 1 o Domain: Housing o Region List: F159.151 • Interface Side 2 o Domain: Rotor o Region List: F100.82, F123.82, Rotor_Inner_Joints • Interface Models o Option: General Connection • Frame Change/ Mixing Model o Option: Transient Rotor-Stator • Pitch Change o Option: None Additional Interface Models • Mass and Momentum o Option Conservative Interface Flux • Interface Model o Option None • Conditional Connection Control Unchecked Mesh Connection • Mesh Connection o Option GGI • Intersection Control Unchecked
Solver	Solution Units	Basic Settings • Mass Units: [kg] • Length Units: [m] • Time Units: [s] • Temperature Units: [K] • Angle Units: Checked o Angle Units: [rad] • Solid Angle Units: Checked o Solid Angle Units: [sr]
Solver	Solver Control	Basic Settings • Advection Scheme o Option: High Resolution • Transient Scheme o Option: 2^{nd} OrderBE • Time step Initialization o Option: Automatic o Lower Courant Number: Unchecked o Upper Courant Number: Unchecked • Turbulence Numerics o Option: First Order

		• Convergence Control
		  o Min. Coeff. Loops 1
		  o Max. Coeff. Loops 5
		  o Fluid Timescale Control
		  ▪ Timescale Control: Coefficient Loops
		• Convergence Criteria
		  o Residual Type: RMS
		  o Residual Target: 1e-4
		  o Conservation Target: Unchecked
		• Elapsed Wall Clock Time Control: Unchecked
		• Interrupt Control: Unchecked
		Equation Class Settings
		• Equation Class: Continuity, Energy, Momentum, Turbulence Eddy Disspation, Turbulence Kinetic Energy
		• Continuity: Unchecked
		Advanced Options
		• Pressure Level Information: Unchecked
		• Body Forces: Unchecked
		• Interpolation Scheme: Unchecked
		• Temperature Damping: Unchecked
		• Velocity Pressure Coupling: Unchecked
		• Compressibility Control: Unchecked
		• Intersection Control: Unchecked

Solver	Output Control	Results • Option: Standard • File Compression: Default • Output Equation Residuals: Unchecked • Extra Output Variable List: Unchecked Backup Results: Blank Trn Results: Blank Trn Stats: Blank Monitor • Monitor Objects: Checked* *Under “Monitor Points and Expressions”, insert: • Monitor Point 1: Enter expression value: torque_z()@Rotor Default to monitor rotor torque. Unchecked “Coord Frame”. • Monitor Point 2: Under “Options,” choose Cartesian Coordinates. Under “Output Variables List,” choose Pressure. Under “Cartesian Coordinates,” enter 0.058m, -0.025m, 0.1021m respectively. Unchecked “Coord Frame” and “Domain Name”.
Define Run	Partitioner	Partitioning Detail • Partition Type: Radial • Partition Weighting: Automatic • Option:Coordinate Axis

		• Rotation Axis: Global Z • Multidomain Option: Coupled Partitioning • Multipass Partitioning: Transient Rotor Stator

THIS PAGE INTENTIONALLY LEFT BLANK

APPENDIX C. INITIAL 4-INCH CFF MODEL

A. DESCRIPTION

The initial model of 4-inch CFF model was created to ensure that helical-bladed CFF would contribute to produce more thrust and power as compared to straight-bladed CFF. The created models for the straight-bladed CFF and the helical-bladed CFF as well as the assembly with the housing were illustrated in Figures 33 to 35 respectively.

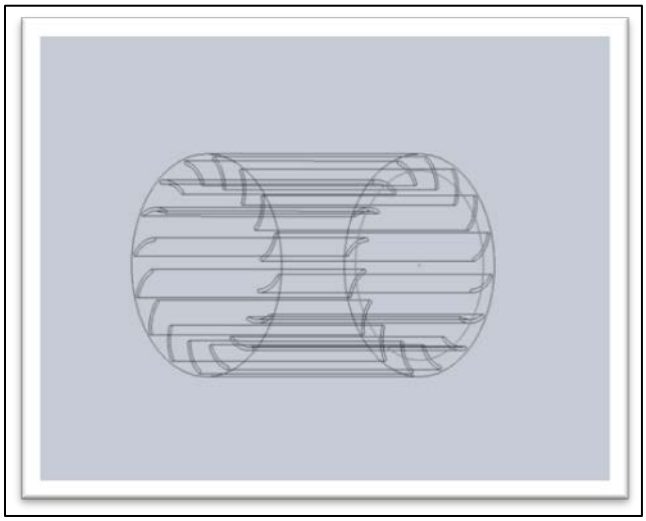

Figure 33. 4-inch straight-bladed CFF

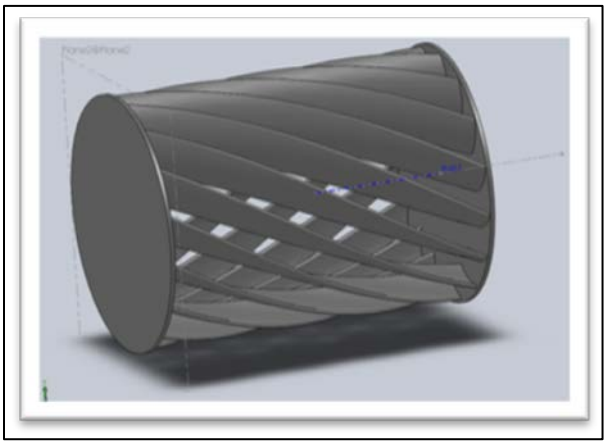

Figure 34. 4-inch helical-bladed CFF

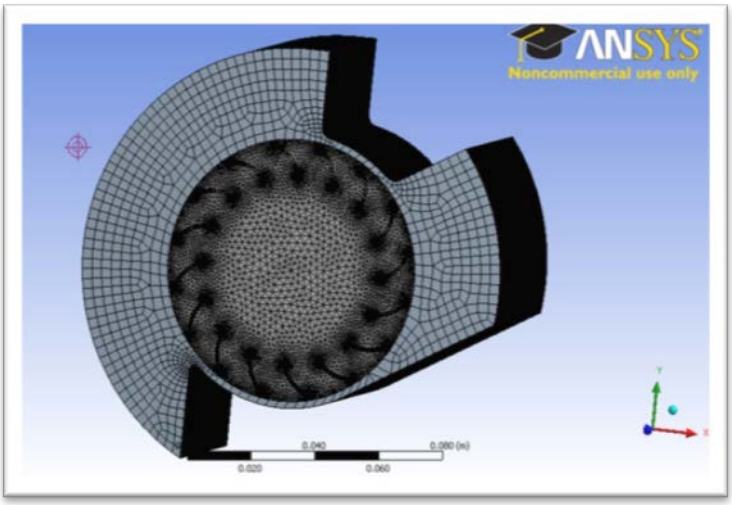

Figure 35. 4-inch rotor and housing assembly

The types of meshes generated are as shown in Table 7. The medium mesh of 2,780,314 nodes and 14,814,742 is used. The fine mesh is not chosen as the difference between the chosen mesh is not significant. Due to the large model created, the required time to complete the simulation run took about 1 to 1.5 weeks and the computational resources required were about 14 processors.

Table 7. Meshes generated for the 4-inch model

		Coarse	Medium	Fine
Rotor	**Nodes**	2,687,202	2,688,298	2,693,972
	Elements	14,734,784	14,738,589	14,771,968
Housing	**Nodes**	75,922	92,016	169,452
	Elements	61,194	76,153	146,832
Total	**Nodes**	2,763,124	2,780,314	2,863,424
	Elements	14,795,978	14,814,742	14,918,800
Difference	**Nodes**		17,190	83,110
	Elements		18,764	104,058

APPENDIX D. RAW DATA FROM DELAGRANGE'S EXPERIMENT

A. DESCRIPTION

Shown in Table 8, was the raw data that Delagrange gathered from his experiments. These data were not presented in his thesis. To have a better appreciation of the power absorbed by the CFF instead of the measured power consumption [11] of the electric motor driving the CFF, Delagrange's raw data were used for the power calculations in the current thesis.

Table 8. Raw data obtained from Delagrange's experiment

Speed (rpm)	Average measured velocity (m/s)	Mass flow (kg/s)	Delagrange's experimental power (W) results
2000	9.1933	0.0574	4.8543
4000	19.9367	0.1246	49.5067
6000	32.4033	0.2024	212.5570
8000	45.7267	0.2857	597.3308

THIS PAGE INTENTIONALLY LEFT BLANK

LIST OF REFERENCES

[1] *Multi-bypass ratio propulsion system technology development*, vol. I-III, Naval Air System Command Contract N00019-74-C0434, Vought Systems Division, LTV Aerospace Corporation, July 24, 1975.

[2] D. H. Gossett, “Investigation of cross flow fan propulsion for a lightweight VTOL aircraft,” M.S. thesis, Department of Aeronautics and Astronautics, Naval Postgraduate School, Monterey, CA, March 2000.

[3] W. T. Cheng, “Experimental and numerical analysis of a crossflow fan,” M.S. thesis, Department of Aeronautics and Astronautics, Naval Postgraduate School, Monterey, CA, December 2003.

[4] C. W. Schreiber, “Effect of span variation on the performance of a cross flow fan,” M.S. thesis, Department of Mechanical and Astronautical Engineering, Naval Postgraduate School, Monterey, CA, June 2006.

[5] H.T. Yu, “Experimental investigation and numerical prediction of a cross flow fan,” M.S. thesis, Department of Mechanical and Astronautical Engineering, Naval Postgraduate School, Monterey, CA, December 2006.

[6] J. M. Ulvin, “Experimental investigation of a six inch diameter, four inch span cross-flow fan,” M.S. thesis, Department of Mechanical and Astronautical Engineering, Naval Postgraduate School, Monterey, CA, June 2008.

[7] S. Cordero, “Investigation of performance improvements including application of inlet guide vanes to a cross flow fan,” M.S. thesis, Department of Mechanical and Astronautical Engineering, Naval Postgraduate School, Monterey, CA, September 2009.

[8] A. J. Gannon, J. M. Utschig, G. V. Hobson, and M. F. Platzer, “Experimental investigation of a small-scale cross-flow fan for aircraft propulsion,” presented at the ISROMAC Conference, Honolulu, HI, February xx, 2006.

[9] V. Antoniadis, “Numerical and experimental investigation of performance improvements of a cross-flow fan,” M.S. thesis, Department of Mechanical and Aerospace Engineering, Naval Postgraduate School, Monterey, CA, June 2010.

[10] J. Krummer, “Propulsive wing,” http://www.propulsivewing.com. Accessed August 1, 2012.

[11] C. T. Delagrange, “Viability of cross-flow fan for vertical take-off and landing aircraft,” M.S. thesis, Department of Mechanical and Aerospace Engineering, Naval Postgraduate School, Monterey, CA, June 2012.

[12] A. J. Gannon, Cheon Ik Jang, G. V. Hobson, K. T. Millsaps, “The effects of blade number and cavities on cross-flow fan acoustics,” presented at the *ISROMAC-14 Conference*, Honolulu, HI, February 27–March 7, 2012.

INITIAL DISTRIBUTION LIST

1. Defense Technical Information Center
   Ft. Belvoir, Virginia

2. Dudley Knox Library
   Naval Postgraduate School
   Monterey, California

3. Chairman, Code ME
   Department of Mechanical and Aerospace Engineering
   Naval Postgraduate School
   Monterey, California

4. Professor Garth V. Hobson
   Department of Mechanical and Aerospace Engineering
   Naval Postgraduate School
   Monterey, California

5. Research Assistant Professor Anthony J. Gannon
   Department of Mechanical and Aerospace Engineering
   Naval Postgraduate School
   Monterey, California

6. COL Lim Soon Chia
   Defence Research and Technology Office
   Ministry of Defence
   Singapore

7. Professor Yeo Tat Soon
   Temasek Defence Systems Institute
   National University of Singapore
   Singapore

8. Ms. Tan Lai Poh
   Temasek Defence Systems Institute
   National University of Singapore
   Singapore

9. Mr. Leo Tin Boon
   Temasek Defence Systems Institute
   National University of Singapore
   Singapore